AFRL-IF-RS-TR-2003-234
Final Technical Report
October 2003

COMPUTATIONAL, EXPERIMENTAL AND ENGINEERING FOUNDATIONS OF IONIC CHANNELS AS MINIATURIZED SENSORS, DEVICES AND SYSTEMS

University of Illinois

Sponsored by
Defense Advanced Research Projects Agency
DARPA Order No. K900

AIR FORCE RESEARCH LABORATORY
INFORMATION DIRECTORATE
ROME RESEARCH SITE
ROME, NEW YORK

This report has been reviewed by the Air Force Research Laboratory, Information Directorate, Public Affairs Office (IFOIPA) and is releasable to the National Technical Information Service (NTIS). At NTIS it will be releasable to the general public, including foreign nations.

AFRL-IF-RS-TR-2003-234 has been reviewed and is approved for publication.

APPROVED:

/s/

CLARE D. THIEM
Project Engineer

FOR THE DIRECTOR:

/s/

JAMES A. COLLINS, Acting Chief
Information Technology Division
Information Directorate

REPORT DOCUMENTATION PAGE

Form Approved
OMB No. 074-0188

1. AGENCY USE ONLY (Leave blank)	2. REPORT DATE	3. REPORT TYPE AND DATES COVERED
	Oct 03	Final Apr 01 – Aug 02

4. TITLE AND SUBTITLE
COMPUTATIONAL, EXPERIMENTAL AND ENGINEERING FOUNDATIONS OF IONIC CHANNELS AS MINIATURIZED SENSORS, DEVICES AND SYSTEMS

5. FUNDING NUMBERS
C - F30602-01-2-0513
PE - 61101E/62712E
PR - E117
TA - 00
WU - 66

6. AUTHOR(S)

Narayan R. Aluru, Robert S. Eisenberg, Karl Hess, Eric Jakobsson and Umberto Ravaioli

7. PERFORMING ORGANIZATION NAME(S) AND ADDRESS(ES)

PRIME
University of Illinois
109 Coble Hall
801 S. Wright St.
Champaign, IL 61820

SUB
Dept of Molecular Biophysics & Physiology
Rush Medical Center
Chicago, IL 60612

8. PERFORMING ORGANIZATION REPORT NUMBER

9. SPONSORING / MONITORING AGENCY NAME(S) AND ADDRESS(ES)

DARPA
3701 N. Fairfax Drive
Arlington, VA 22203

AFRL/IFTC
26 Electronic Pky
Rome, NY 13441-4514

10. SPONSORING / MONITORING AGENCY REPORT NUMBER

AFRL-IF-RS-TR-2003-234

11. SUPPLEMENTARY NOTES

AFRL Project Engineer: Clare Thiem, IFTC, 315-330-4893, thiemc@rl.af.mil

12a. DISTRIBUTION / AVAILABILITY STATEMENT

Approved for public release; distribution unlimited.

12b. DISTRIBUTION CODE

13. ABSTRACT ***(Maximum 200 Words)***

Continuum and Particle methods were employed to simulate ion channels to study their characteristic properties like ion permeation and selectivity in order to demonstrate ion channels as biosensors. Fast, efficient and accurate simulators for modeling the conduction, selectivity and sensitivity of ionic channels have been developed. The continuum simulators were based on 3-D Poisson-Nernst-Planck (PNP) theories and stochastic dynamics. The transport coefficients and parameters (such as mobility, diffusivity, permittivity, etc.) were extracted from molecular dynamic simulations and from experimentation. The continuum theories are being tested by extensive experimentation to establish the range of validity of the PNP theories. A multiscale approach that involves fine-grained calculations (molecular dynamics) at atomic detail was developed to calculate the mobility of individual ions and the forces that ions are subject to in passage through the channel, and coarse-grained calculations to compute the actual fluxes. The fine-grained calculations are molecular dynamics and electrostatics. The coarse-grained calculations are stochastic dynamics (a variant of Monte Carlo) and PNP model. Models to mimic ion channels have been explored by using functionalized carbon nanotubes in molecular dynamics simulations. Quantum corrections to van der Waals interactions were also computed to explore these in more detail. Experimental effort provided data on porin and its mutants which will be validated with simulation tools in the future using this data.

14. SUBJECT TERMS
Ion channels, Poisson-Nernst-Planck (PNP) theory, molecular dynamics, continuum theory, stochastic simulation, van der Waals interactions, porin, selectivity

15. NUMBER OF PAGES
52

16. PRICE CODE

17. SECURITY CLASSIFICATION OF REPORT	18. SECURITY CLASSIFICATION OF THIS PAGE	19. SECURITY CLASSIFICATION OF ABSTRACT	20. LIMITATION OF ABSTRACT
UNCLASSIFIED	UNCLASSIFIED	UNCLASSIFIED	UL

TABLE OF CONTENTS

LIST OF FIGURES

ACKNOWLEDGMENTS

The Principal Investigators would like to thank Dr. Anantha Krishnan, Program Manager, Defense Advanced Research Projects Agency (DARPA), Defense Science Office (DSO), and Mr. Clare Thiem, Laboratory Program Manager, Air Force Research Laboratory (AFRL), Advanced Computing Technology Branch (IFTC) for useful suggestions.

1 EXECUTIVE SUMMARY

A study funded by DARPA, was conducted to understand the mechanism of transport in ion channels and their possible application as single molecule detection sensors. This report details the motivation for such a study, the various approaches used and the results obtained so far. In this project, a 3-D Poisson Nernst Planck approach using PROPHET to simulate ion channels like porin was demonstrated for the first time. Techniques and tools were developed to obtain experimental data for ion channels – specifically porin. Continuum equations that predict selectivity, sensitivity, and gating based on mean field theories have been demonstrated for two channel types of different structure. Channel types of same structure have not yet been compared in detail. Multi-scale simulations that predict selectivity and sensitivity have been started and early work has been completed and published. This is the first time that multiscale simulations have been done for ion channels. Gating has not yet been analyzed. Experiments showing how well porin and its mutants are described by continuum theories and by multi-scale simulation are finished on two mutants and well underway on two others, of known structure. The sensitivity of porin to mutation and ion binding has been established showing its feasibility as an ion sensor.

Major Findings:

- Currents have been measured in a single protein molecule of known structure in a wide range of solutions. Previous measurements were made in an ensemble of channels of unknown orientation and number, preventing quantitative analysis.
- Currents have been compared among continuum *PNP* models in three different and independent versions and experiments. This is a tremendous increase in understanding because no one before had used a theory in which electrical potential was computed from Maxwell's equations.
- Currents have been compared among four models of selectivity and the currents observed in three channel types (Ca^{++}, Na^{+}, and Cl^{-} : K^{+} is in progress) in a wide range of conditions. This is an enormous increase in capability since no physical theory has matched more than one or two of these observations.
- Simulations have shown the existence of a discrete water switch in carbon nanotubes which is being sought experimentally right now. This is a qualitative change in understanding.
- Simulations have shown how to put ions into carbon nanotubes which is being sought experimentally right now. Simulations have shown that chemical functionalization of the mouth of carbon nanotubes can give it properties like selectivity in an ion channel. This is a new observation which has lot of potential for further studies.
- Simulations have shown how to embed molecular dynamics data into continuum models. Such an approach is very helpful to bridge the time scale and length scale

gap between Molecular Dynamics simulations and continuum simulations. This is a qualitative change in understanding.

- Standard code of computational electronics has been used to predict ion movement through channels. Electronics and ionics stand united, for the first time, as far as we know.
- Self consistent simulations of ion movement (in which the electric field is computed directly from Poisson's equation) have been made to predict ion movement through gramicidin channels. Transport Monte Carlo has been implemented for channels.

2 INTRODUCTION

Ion channels are powerful device components with numerous biological functions. They are the molecular basis for the movement of electrical currents across membranes, resulting in signal transduction. Detecting pathogens, for instance, means selecting some unique feature associated with them, and then creating an easily measurable signal, such as an electrical current, of that detection. The key features of ion channels that give rise to their extraordinary range of biological functions include variations in: 1) their **selectivity** (what ions can pass through), 2) their **conductance** (how rapidly can ions get through), and 3) their **sensitivity** (how the conductance is modulated by such factors as the chemical composition of their environment, the transmembrane voltage, the membrane surface tension, and the chemical binding of the ion, etc.). Some of the various biological functions of channels that potentially have enormous significance for device design and engineering include:

Signaling and computation--Ion channels are the current carrying and regulatory molecules of the nervous system, required for diverse purposes, including sensory input, cognition, coordination of motion, and general housekeeping functions of the body. As elements for computation, ion channels are not as fast as solid state devices; however, assemblies of ion channels as organized in neuronal membranes are capable of very complicated and specific input-output patterns. This presumably is the basis for the brain's excellence in pattern recognition and in the coordination of complex motions, capabilities not close to being matched by human-constructed computers or electronic devices.

Triggers for cellular events--Many cellular processes are triggered by electrical signals generated at the cell surface by ion channels. This includes, but is not limited to, muscle contraction, glandular secretion, and sperm entry into the egg.

Electrical power generation--Some species of fish have electric organs that produce large pulses of electrical energy which stun prey in the nearby water. The source of the electrical current and voltage is ion channels in membranes that are stacked in series with each other, much as cells in a car battery. Selective ion channels act as molecular batteries that transduce the chemical potential of the ionic species for which they are selective into an electromotive force that can drive electrical current.

Energy transduction--Proton channels are critical components of the molecular apparatuses for transducing energy from photons (light) into a form that can be used for nutrient synthesis in plants. Proton channels are equally important in the exchange of energy between ATP and other forms of useful chemical energy in the cell. The ATP synthase enzyme, which contains in one protein assembly both a proton channel and catalyst for the reaction between ATP, ADP and free P_i, is almost 100% efficient and reversible. Depending on the proton gradient across the membrane and the ATP/ADP/P_i ratio, it can use the proton gradient to synthesize ATP or use an ATP surplus to pump protons with essentially the same stoichiometry.

Fluid pumping and filtration--The universal mechanism for moving fluid and electrolytes across boundaries in organisms is via osmotic pressure created by regulated ion movement through channels. For example, channels regulate the flow of water across the airway epithelium to keep it moist, and across the intestinal epithelium to regulate water content in the bowels. Cystic fibrosis is an ion channel disease which results in a deficiency in the movement of water across the airway epithelium, and cholera is a lethal disease caused by the misregulation of ion channels in the intestinal epithelium. Another vital example of this aspect of channel utility is the function of the kidney. A dramatic example of the movement of fluid via osmotic pressure can be observed in root cells which provide water to the tops of the highest trees. (Indeed, it seems that the osmotic pressure available from physiological electrolyte (about 300 milliosmolar) is a fundamental limitation of tree height.)

Chemical sensing--Ion channel proteins often contain domains that are selective for various chemical species, and are gated by binding with those species. For example, chemically sensitive ion channels are responsible for taste sensing in the tongue and palate.

Mechanotransduction--Ion channels are responsible for mechanosensitivity in cells. It has been shown that some bacterial channels open and close in response to surface tension changes in the membrane in which they are embedded. In other cells, the opening and closing of ion channels which sense mechanical deformation are mediated by changes in cytoskeleton tension, rather than the membrane directly.

In summary, ion channels in nature are integral components of a myriad of biological processes and functions that have clear counterparts in human technology. Engineered ion channels are thus potentially useful components in micro- and nanotechnology applications.

In this project a three-pronged approach to build the foundations of ionic channels as engineered devices for innovative technological applications was pursued. A team of experts to address the computational, experimental and engineering (or fabrication) aspects of ion channels was assembled. Specifically, the team developed some of the first simulation tools, in close collaboration with the experimental effort, for multi-scale and mixed-domain (electrical, chemical, biological and microfluidic) analysis of ion channels to obtain fundamental insights into the selectivity, conductivity, and sensitivity of ion channels [19], [6]. The approach is summarized in Figure 1. The simulation effort relies heavily on the experimental and fabrication effort to extract transport coefficients and the structure of the channel, respectively. Once the accuracy of the transport models in ion channels has been established, the simulation tools will enable speculative design of miniaturized devices and systems. The validation of the simulation enabled speculative designs will be established by the experimental and engineering effort.

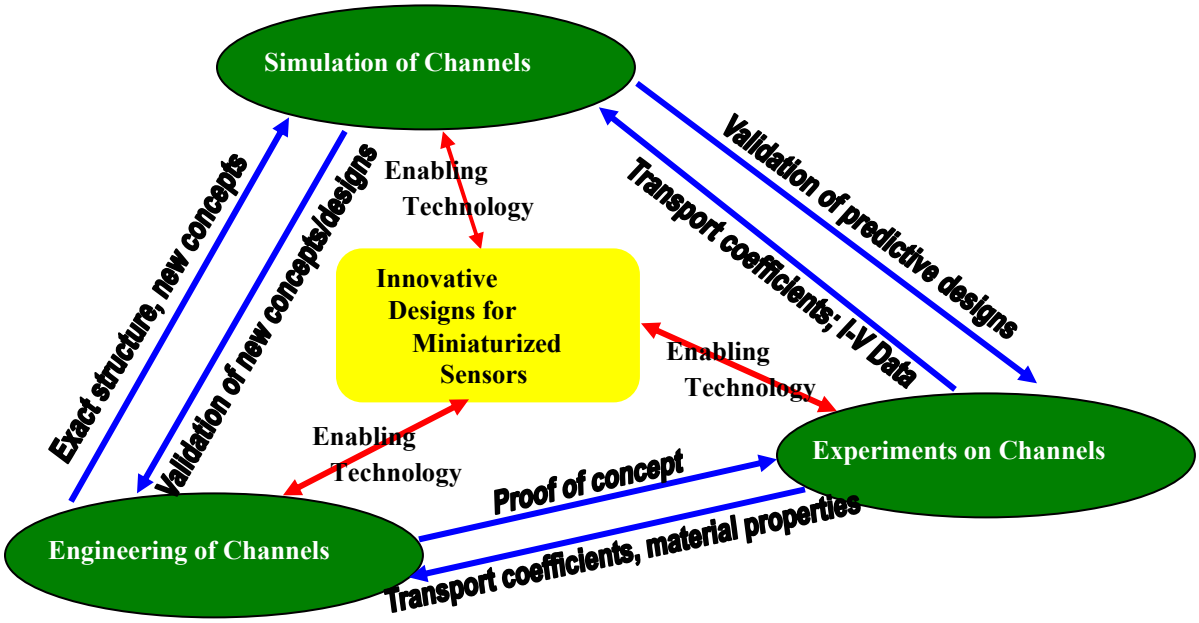

Figure 1. A three-pronged approach to enable design of innovative technology based on ion channels

As shown in the figure above, the goal of our project is to demonstrate Ion Channels as Biosensors**.** This goal involves several tasks, which are summarized below:

Task 1: Continuum simulators for ionic channels based on mean-field theories

1.1 Develop fast and efficient simulators for steady-state analysis of continuum model for extraction of I-V curves.
1.2 Create reduced-order models for fast dynamic analysis of the continuum model
1.3 Establish accuracy of continuum models
1.4 Calibrate transport coefficients for predictive design

Task 2: Molecular and multiscale modeling of ionic channels

2.1 Develop molecular dynamics (MD) techniques for simulation of ionic channels
2.2 Conduct Monte Carlo (MC) and combined MC/MD analysis of channels
2.3 Extract transport coefficients such as permittivity, diffusion coefficients etc. from molecular analysis
2.4 Conduct multiscale (combined continuum/molecular) modeling of ionic channels

Task 3: Simulation of gating phenomena to enable simulation driven innovation of chemical and biological sensors

3.1 Perform continuum modeling of various gating phenomena
3.2 Conduct molecular modeling of various gating mechanisms.

3.3 Utilize different simulation and experimental approaches to obtain fundamental insights into selectivity and sensitivity of ion channels.

Task 4: Experimental effort on ionic channels

4.1 Obtain I-V data for gramicidin, porin, and other channels to enable accuracy of simulation tools
4.2 Obtain experimental data on transport coefficients
4.3 Perform experiments on speculative designs enabled by simulation tools

The following pages summarize the results of the project. The first part of the report is on different simulation approaches for characterizing ion channels. In sections 3, 4 and 5 results from Drift Diffusion, Monte Carlo and Molecular Dynamics simulations are discussed. In section 6 a summary of the theory and experimental results to understand selectivity is given. In the second part results from investigations on the possibility of incorporating the functionality of ion channels into carbon nanotubes are reported. Section 7 is on Molecular dynamics simulations of carbon nanotubes in electrolytes and Section 8 is on Quantum correction to potentials used in molecular dynamics simulations of Carbon nanotubes. The appendix has two key articles published due to this project which have the relevant mathematical equations.

3 CONTINUUM THEORY: DRIFT DIFFUSION SIMULATIONS OF PROTEIN CHANNELS

Continuum theories are based on a flow model that solves for the transport of an equivalent fluid representing the macroscopic properties of the actual particle flow. Self-consistent continuum models include continuity equations for the density of each ionic species, and the Poisson equation in linear or nonlinear form, depending on the approach used for the solution. The flow model can be derived starting from the Langevin transport equation or the Boltzmann transport equation. In both cases, similar assumptions must be made of carrier distributions near equilibrium, and an identical current equation with a drift and a diffusive term is obtained. The resulting system of equations constitutes the Poisson-Nernst-Planck model of transport, which is the ionic equivalent of the drift-diffusion Shockley equations used in semiconductor devices for electron and hole transport. The continuum approach has the advantage of fast solution methods, and good flexibility if complicated geometries must be accommodated. Therefore, it is very suitable to explore the qualitative behavior of structures, by varying a vast parameter space, fast and efficiently. In addition, the transport model is based on one main parameter (mobility or diffusivity) which can be readily calibrated to account for higher order effects. Continuum models are also necessary to formulate compact or reduced-order models for the study of arrays of elements. For structures which are as small as ionic channels, however, one has to keep in mind that this class of models provides a description of the behavior which is correct, in an average sense, at the terminals. The carrier densities obtained inside the structure need to be interpreted as long-time steady-state averages at each location, and are not representative of ionic charge configurations, which might be established at any one instant of the transport process. The same consideration holds for the currents, which are time-average and do not resolve the fluctuations exhibited by the particle flow. Still, continuum models are the corner stone of an effective hierarchical simulation strategy and can be efficiently calibrated from measurements or higher-order models. A great advantage of this class of approaches is that complicated phenomena, like ion binding and release on the wall of the pore, can be represented fairly easily in terms of generation-recombination terms and trap sites, with almost no consequence in the overall numerical complexity.

A framework for three-dimensional (3D) drift-diffusion simulations of ion transport in protein channel systems has been developed, based on the simultaneous solution of Poisson's equation [2],[8]. The detailed derivation of the PNP equations are given in [17]. This concept describes coulomb interactions between all mobile and fixed charges, and a continuity equation for each ion species, describing ion permeation down an electrochemical gradient. Water, protein and lipid are treated as continuum regions characterized by specific dielectric constants. Macroscopic current flow is resolved by assigning an appropriate mobility and diffusion coefficient to each ionic species.

The drift-diffusion model is implemented using PROPHET, a robust commercial simulation platform based on state-of-the-art numerical engines. The correctness of the solvers and of the simulation models have been exhaustively tested and validated over at

least two decades by industrial and university groups. The non-linear solution procedure uses a robust Newton iteration, and discretization of the flux equations uses the correct exponential interpolation realized by the Scharfetter-Gummel approximation.

The drift-diffusion model has been used to calculate the current-voltage characteristics of several ion channels, including OmpF porin and some of its mutants, in various electrolytes [1].

The PROPHET simulator has been used to compute the open channel current-voltage (*IV*) curves for wild-type porin *OmpF* and its mutant *G119D* in a range of solutions of KCl and $CaCl_2$ [3], [4]. It is straightforward to include several multi-valent species in the PROPHET framework without modifying the source-code. For the purpose of matching current-voltage measurements at the system level, the channel is treated as a "black box" and a spatially uniform diffusion coefficient is used as the fitting parameter. A selection of the results obtained using a spatially uniform diffusion coefficient is shown in figures 2 and 3.

The mutation of wild-type *OmpF* to *G119D* increases the negative charge and further narrows the cross-section of the constriction region of each pore of the trimer. Experimentally, the conductance of *G119D* is seen to be 15-40% lower than the wild-type. PROPHET was used to study the effects of the stearic and electrostatic changes introduced by the mutation, separately. Figure 4 shows that the current-voltage curves of *G119D* computed both with and without the extra $-3|e|$ charge are almost identical. This suggests that the reduced conductance of the mutant is due to a narrowing of the pore constriction rather than changes in the distribution of permanent charge that accompany the mutation.

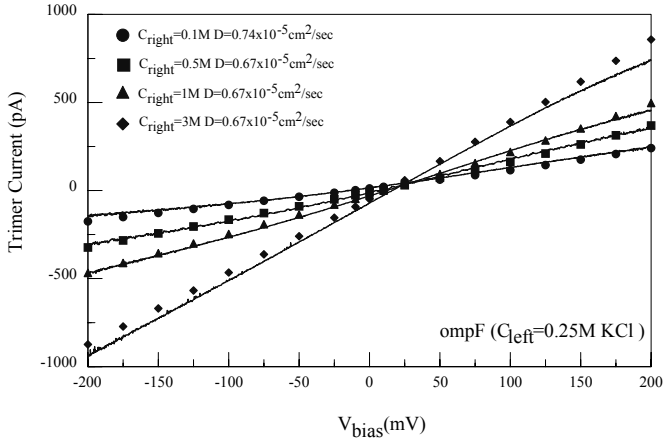

Figure 2. Experimentally measured and computed current-voltage curves for OmpF in asymmetric solutions of KCl: 0.25:0.1M, 0.25:0.5M, 0.25:1M, 0.25:3M. A single spatially uniform diffusivity D, adjusted to give the best fit to the measured curves, was used.

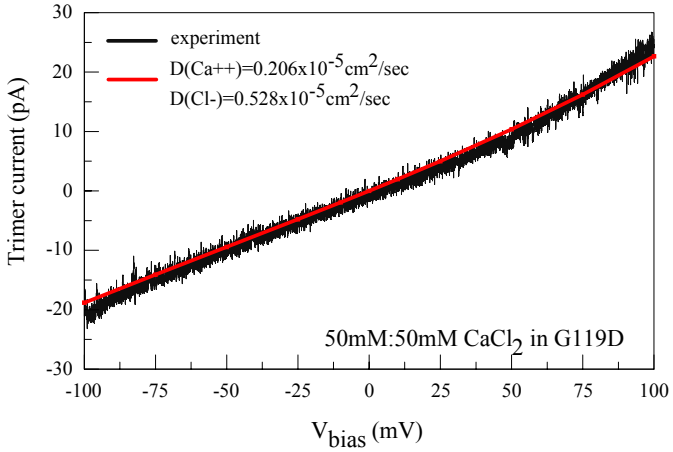

Figure 3. Experimentally measured and computed current-voltage curves for G119D in 50mMCaCl2. The diffusivity of each species was adjusted to give the best fit to the measured curves.

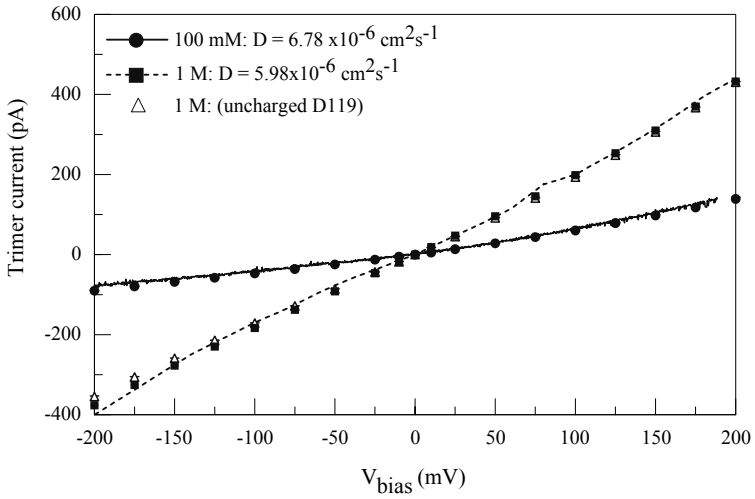

Figure 4. Comparison of drift-diffusion model with measured current-voltage curves for *G119D* in 100mM and 1M KCl. Measured data are indicated with solid (100mM) and dashed (1M) lines, the simulation data are indicated with symbols. The current-voltage curve obtained using the *G119D* and the charge distribution of wild-type OmpF (Δ) is almost identical to that of *G119D* (■).

The PROPHET framework for specifying an arbitrary space-dependent diffusivity for all ion species is now complete. Experimentally known ion diffusivities can be applied in the bulk-electrolyte regions and coupled with values that vary within the channel pore, inferred either from higher order physical models (e.g., Molecular Dynamics) or from fitting the measured current-voltage curves. Fitting of experimental curves using a more physical model of diffusivity is inherently more difficult due to the restricted tunability of the parameter space.

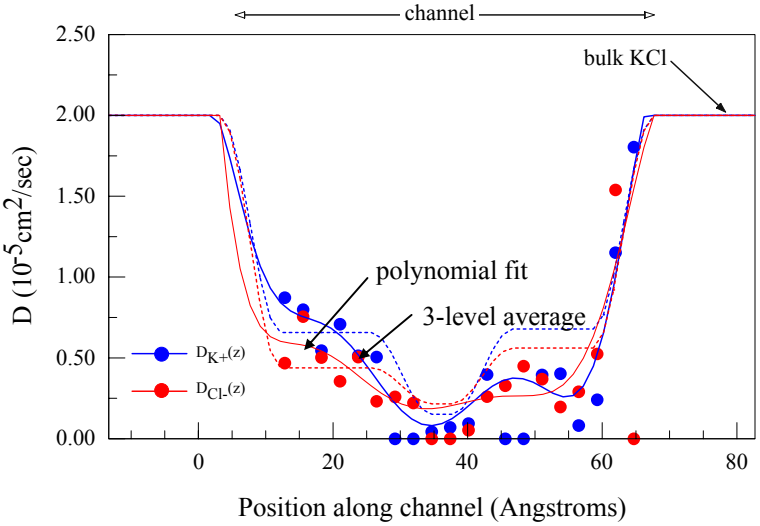

Figure 5. Diffusion coefficient profiles for K^+ (blue) and Cl^- (red) along the OmpF porin channel inferred from mean-square-deviation calculations of Molecular Dynamics (symbols) together with a polynomial fit (solid lines) and 3-level average fit (dashed lines).

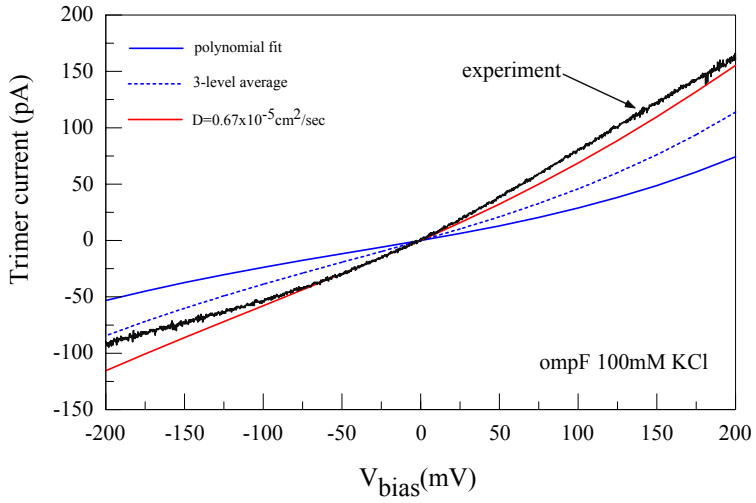

Figure 6. Current-voltage curve measured for OmpF in 100mM KCl compared with current-voltage curves computed using (i) two diffusivity profiles shown in Figure 5 (polynomial and 3-level average fits to MD data) and (ii) uniform diffusion coefficient.

4 PARTICLE METHODS: MONTE-CARLO SIMULATION OF ION CHANNELS

The accuracy of continuum theories is questionable for nanoscale systems such as ion channels, especially when experimental data is not available and diffusion coefficients cannot be calibrated easily. To address this issue, we have developed both Monte Carlo and Molecular Dynamics approaches for ion channels.

Conduction in ion channels has many similarities with transport in ultra-scale semiconductor devices with granular doping. We have adopted Monte Carlo device simulation strategies to pursue the study of ion channels from a device engineering point of view. This was accomplished by coupling solution reservoirs to the conducting channel, and by treating the movement of ions self-consistently in 3-D. Our previous work indicated that main problem in the simulation of ionic channel conduction is that for an ion, successful traversal of the channel is a rare event. Many attempts of ion injection take place, but the vast majority of particles tend to return back to the original solution reservoirs at the ends of the channel. The microscopic particle current is not uniform on short time intervals, and simulations must be extended to millisecond scale to approach the averaging that takes place in a measurement of channel conduction. At the same time, due to the extremely small sizes and the strong Coulomb forces, the time step must be on the order of femtoseconds for a correct resolution of the semi-classical trajectories. Typical semiconductor device models require tens of thousands of particles but reasonable results are obtained in several picoseconds of simulation. Therefore, the ionic channel transport problem is also multiscale in time. Monte-Carlo computational tools serve an important function by bridging the gap between fast continuum simulations and molecular dynamics simulations.

A Transport Monte Carlo code has been developed to simulate ion transport in electrolytes as a sequence of trajectories interrupted by random scattering events. Ion trajectories evolve in three-dimensional space according to a detailed electric field distribution, obtained self-consistently by solving Poisson's equation on a discrete grid. Ion positions are mapped to the grid to generate a spatial distribution of charge density, which provides the right-hand side of the discretized Poisson's equation. Discretization of Poisson's equation leads to a truncation of short-range electrostatic forces. Short-range charge-charge interactions are included explicitly, by evaluating the Coulomb force within a sub-domain surrounding the particles, which is then added to the Poisson equation force (particle-mesh). A correction term to eliminate double counting in the overlap region between the two domains is also required. Ion size is introduced by including a Lennard-Jones interaction potential for ion-ion interactions, and a hard-sphere model potential for impervious boundaries. This creates an additional force that prevents unphysical ion coalescence.

Ion-water electrostatic interactions are handled implicitly by assuming the water to be a continuum background with a given dielectric permittivity. Other types of ion-water interactions are treated stochastically using a scattering rate. The duration between scattering events is obtained by selecting a random number, uniformly distributed on the unit interval. The implicit water model greatly reduces the ensemble size compared to

traditional Molecular Dynamics simulations, enabling the simulation times to extend to 100s of nanoseconds.

The Transport Monte Carlo code is currently being used to study ion transport through the gramicidin channel. Figure 7 shows the representation of the gramicidin channel used in the 3D Transport Monte Carlo model. Electrolyte, protein and lipid are represented by the blue, green and red regions of the domain, respectively. Electrodes, in contact with the electrolyte, are placed at the right and left extremities of the domain, to maintain a fixed bias voltage that drives the ion current. The trajectory of a single Na^+ ion trajectory crossing the channel, under a 250mV bias, is shown. Ion trajectories that cross the channel are extremely rare events. In this 5ns simulation in 1M NaCl only two Na^+ ions were observed to cross the channel. No anions were observed to enter or cross the channel, because their larger ionic radius, which is comparable to the average channel radius. When ion radius is ignored both Na^+ and Cl^- ions can traverse the channel, although the electrostatic barriers presented by the particular configuration of fixed charge lining the pore of the gramicidin channel limits the fraction of current carried by Cl^-.

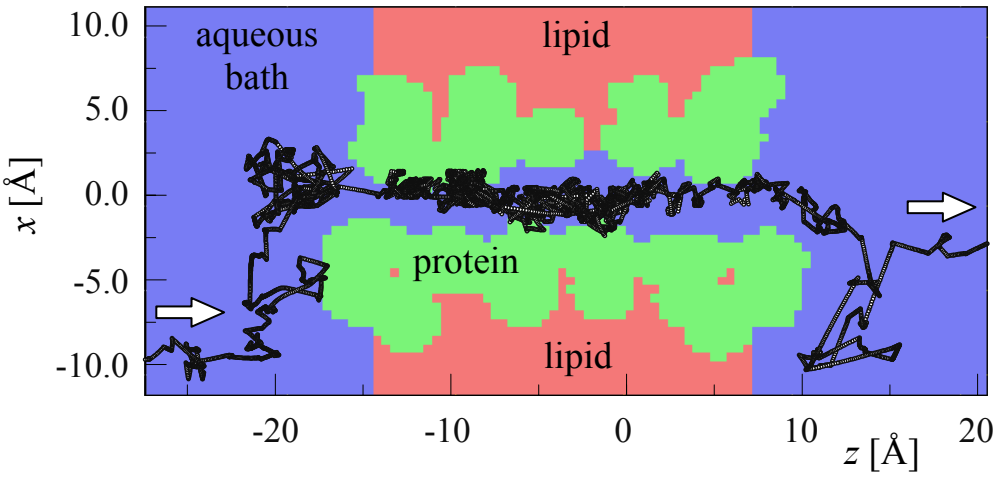

Figure 7. Transport Monte Carlo Simulation of NaCl in gramicidin

5 MOLECULAR DYNAMICS SIMULATIONS OF ION CHANNELS

The finest-grained level of description feasible for describing biomolecular dynamics is as a set of charged balls (the atoms), connected by springs (the bonds). The charges on the atoms, the polarizability of the atoms, the sizes of the atoms, and the energetics of deforming the bonds are collectively known as the force field of the system. Force fields for biomolecular simulations are derived partly from spectroscopic studies on small molecules that are essentially parts of macromolecules, partly from quantum mechanical calculations, and partly are adjusted to fit known constitutive behavior, such as self-diffusion coefficient, dielectric constant, etc. Computing molecular dynamics trajectories is conceptually simple, since atoms simply move according to Newton's laws, but is computationally quite complex, because of the large number of atoms in biomolecular systems and near environment, and the various types of forces involved. There are several programs that are conveniently organized to simulate biomolecular systems. Three of the most commonly used are: AMBER, GROMOS, and CHARMM--our laboratory uses GROMOS.

Given a structural molecular model of a biomolecule, the essence of a molecular dynamics simulation is to assemble the model molecule (i.e., assign spatial coordinates to each atom in the molecule) together with as much of the environment as is needed to provide realistic behavior, initiate thermal motion by assigning random velocities to the atoms with a Maxwellian velocity distribution characteristic of the temperature at which the simulation is to be run, and then let the system move according to Newton's laws. By collecting statistics on the motions, conformations, and the energetics of the system as it moves, one attempts to gain insights into the relationship between the molecular structure and its function.

A Molecular Dynamics study of ion permeation in OmpF porin embeded in 1 M KCl Hydrated Palmitoyloleoylphosphatidylcholine Bilayer was performed [5],[6],[24]. The system under molecular dynamics (MD) simulation consists of a trimer of OmpF, 633 Palmitoyloleoylphosphatidylcholine (POPE) lipid molecules, 626 K^+ cations, 592 Cl^- anions, and 33283 water molecules (i.e., ca. 1 M KCl). The ionization states (distribution of charges in ionizable residues) in porin were calculated with an extended theory which includes the effect of dielectric constant on the shifts of pKa values. An important feature from these pKa calculations is that ASP312 is deprotonated. This is in contrast to earlier model (with ASP312 protonated) used in MD simulation. The system has a total number of 144333 atoms. MD was carried out by the particle-mesh-Ewald method. The simualtion time including equilibration is 6.5 ns. Figure 8 shows a snapshot of the system.

Diffusion coefficients as a function of the z-position (along the bilayer normal) for K^+, Cl^-, and water were calculated from the MD trajectories. They are, respectively, displayed in Figures 9, 10, and 11. From these figures, it is obvious that the mobilities of the ions as well as water inside the pore are smaller than those outside the pore region. The length of the pores span from ca. z = 1.7 nm (intracellular side) to ca. z = 7.2 nm (extra cellular side). Based on the current statistics, the z-profiles of diffusion coefficients and ion densities may not be meaningful to draw conclusions on ion selectivity and permeation.

An alternative approach is to apply voltages across the membrane in the MD simulations. A preliminarily investigation of the feasibility for such a MD simulation was completed. Movies for ion translocations across the channel are posted at <http://peptide.ncsa.uiuc.edu/~schiu/porin.html>

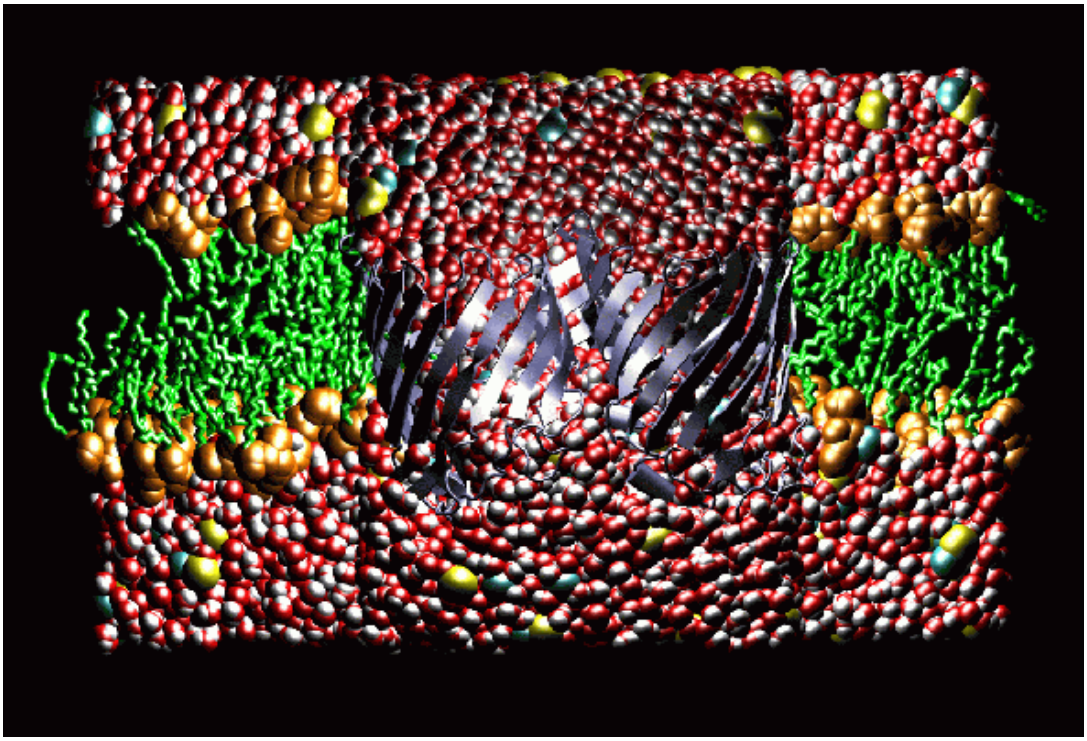

Figure 8. A snapshot of OmpF in POPE from MD simulation

In the future, current-voltage (I-V) curves will be calculated from MD simulations (with various voltages applied across the membrane) for OmpF porin and its mutant G119D. The results from these series of MD simulations may give a better insight into ion selectivity and permeation of porins.

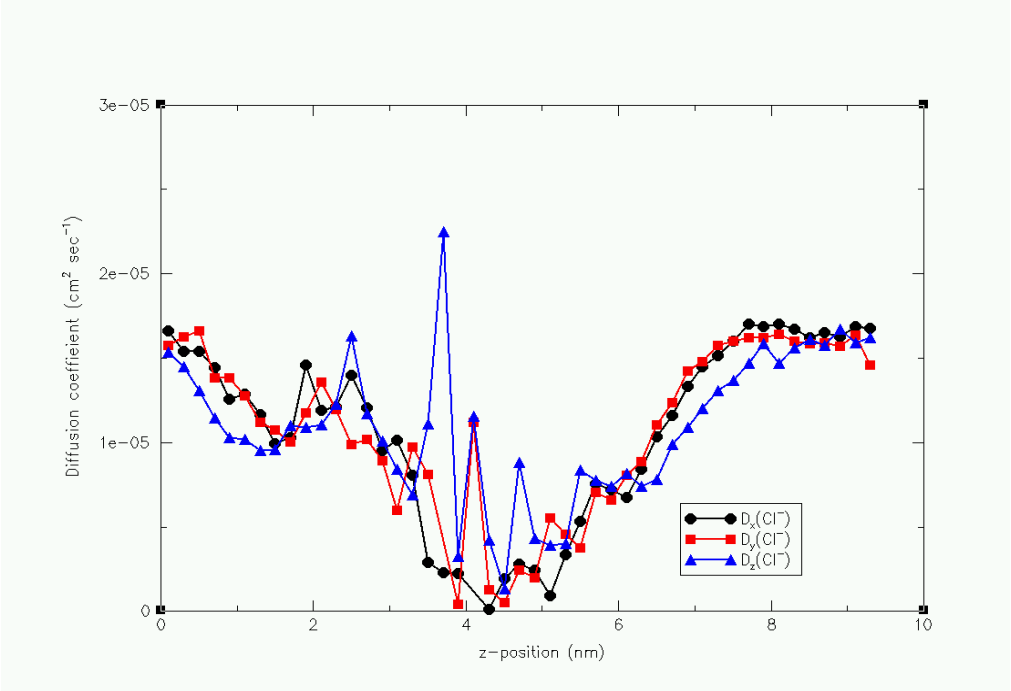

Figure 9. Diffusion coefficient profile for Cl^- ions.

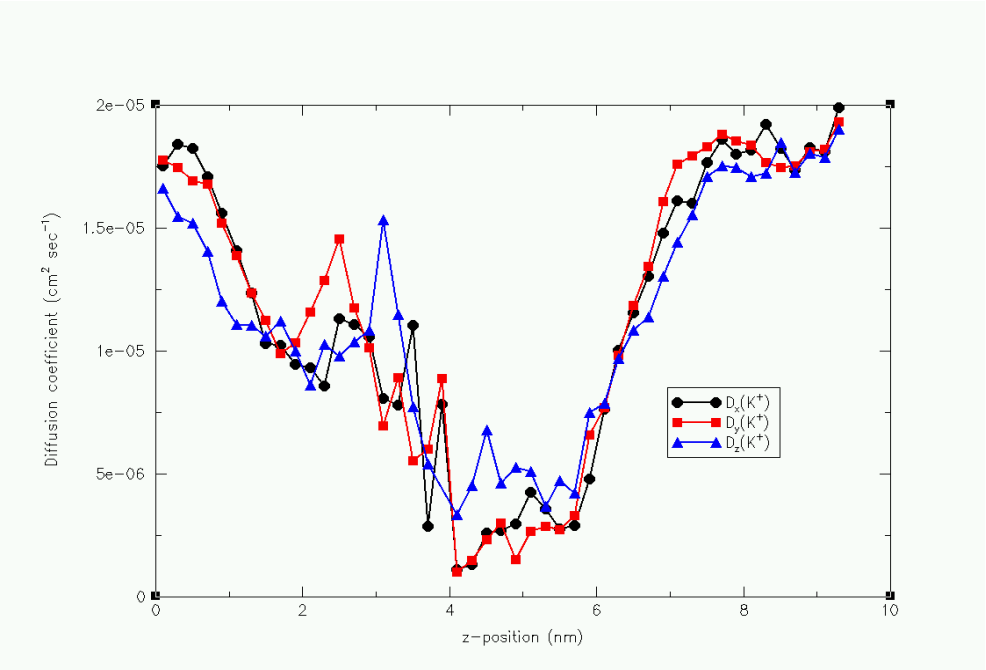

Figure 10. Diffusion coefficient profile for K^+ ion.

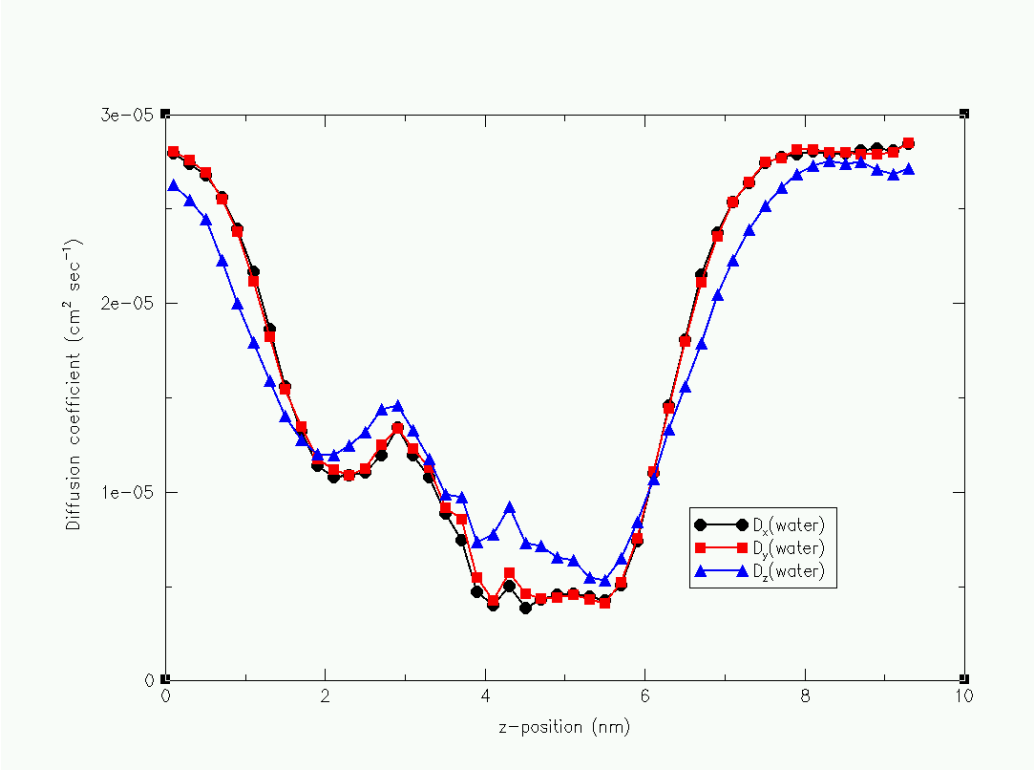

Figure 11. Diffusion coefficient profiles for water.

6 THEORY, SIMULATIONS AND MEASUREMENTS OF SELECTIVITY

A systematic attempt has been made to understand selectivity of the open channel using the methods of the physical chemistry of concentrated salt solutions. Computation and analysis of a system as complicated as an ionic channel requires tight integration between theory, simulation, and experiment [23]. If theory and simulation are not integrated closely with experiment in biophysics, it is easy to do irrelevant work. The simulation and experimental approaches were validated to the best extent possible.

Theory of selectivity:

The first contribution was to use the simplest model of concentrated salt solutions that fits data (i.e., activity coefficient) over the entire range of concentrations, namely the Mean Spherical Approximation (*MSA*). The *MSA* was used to analyze and then predict behavior the *L*-type Ca^{++} channel [21]. This channel was chosen because it is very selective, thus providing a severe challenge to a theory, and has been studied in considerable experimental detail, thus providing another severe challenge to a theory. The channel has also been well characterized by molecular genetics, although its structure is not known. Finally, the *L*-type Ca^{++} channel is among the most important channels in an animal because it controls the heart beat.

The *MSA* theory was successful in fitting a large fraction of the experimental data on selectivity of the *L*-type Ca^{++} channel using just two adjustable parameters (dielectric constant and channel volume) held at fixed values.

Monte Carlo (*MC*) simulations were used to check the MSA theory, which represent the state of the art in the study of homogeneous and inhomogeneous ionic solutions, to check the results of the *MSA*. The results checked. Thus, water was added into the model, using the solvent primitive model (*SPM)* to compute selectivity. The *SPM* not only confirmed the *MSA* and *MC* results but also was able to fit a range of data (e.g., Mg^{++}) that had not been adequately fit previously [16].

Work was begun during this period on the Density Functional Theory of selectivity, as well as on the Na^{+} channel and the Cl^{-} channel [22].

Measurements of selectivity:

An experimental setup has been completed which allows measurement of single channel currents from one channel molecule in a wide range of solutions. The apparatus to change solutions on both sides of the channel has allowed 13 solutions changes on a single molecule in the best situation. It is nearly 100% reliable when making changes on just one side and is about 40% reliable when changing solutions on both sides. The failure

mode is the rupture of the membrane, which is believed to be caused by electrical and not mechanical transients.

This apparatus allowed speedy measurements of the current-voltage (*IV)* relations of porin in some 15 KCl solutions of various concentrations over a voltage range of ±200 mV. This data set is now the mother lode of experimental data of *IV* relations on channels that must be fit by any theory of permeation or selectivity [21]. Experiments were started with other ions.

Theory of Permeation:

The Poisson Nernst Planck (*PNP)* was extended to three dimensions using the spectral element . Several papers were published showing that a direct calculation of current voltage (*IV*) curves was possible and successful [14], [15], [17], [18], [20]. This represents the first use of spectral elements (and perhaps of finite elements) to a channel problem.

Nonequilibrium Statistical Mechanics:

A fundamental problem underlying all modeling of ion channels, and much modeling of proteins, is the correct formulation of statistical mechanics of nonequilibrium systems. Work has been started on a formulation of statistical mechanics using trajectories, not states as the fundamental item being counted. Subsequent work (after the agreement period) has shown that this approach promises to allow a general application of the modern theory of stochastic processes to nonequilibrium statistical mechanics.

7 ION CHANNEL BASED CARBON NANOTUBE SENSORS

Molecular dynamics (MD) has been used to study the possibility of using carbon nanotubes as "ion channels" i.e. incorporating the functionality of ion channels in carbon nanotubes and thereby developing nanopore sensors for single molecule detection. Though carbon is hydrophobic MD simulations show that water enters the nanotube. The diffusion rate of ions into the tube is very low but in the presence of an external electric field, ions enter the carbon nanotube. Additionally, simulations show that the property of selectivity found in "ion channels" can be mimicked by chemical functionalization of the ends of the tube. Currently studies are being done to simulate these under biophysical conditions.

Transport of molecules through macromolecular pores is of considerable importance in many biological and nano-electromechanical systems. In recent years engineered ion channels have been developed to function as single molecule detection systems. Figure 12 shows an engineered ion channel sensor. In an applied potential, an ionic current is carried by the ions that bath both the sides of the lipid bilayer. When the target molecule binds to the binding site in the pore, the current is modulated as shown in the trace. The frequency of binding reveals the concentration of the analyte and the duration and amplitude of the events reveal its identity. Though they have significant advantages including high sensitivity, wide dynamic range and biocompatibility, their lack of durability makes them reliable only in a lab setting.

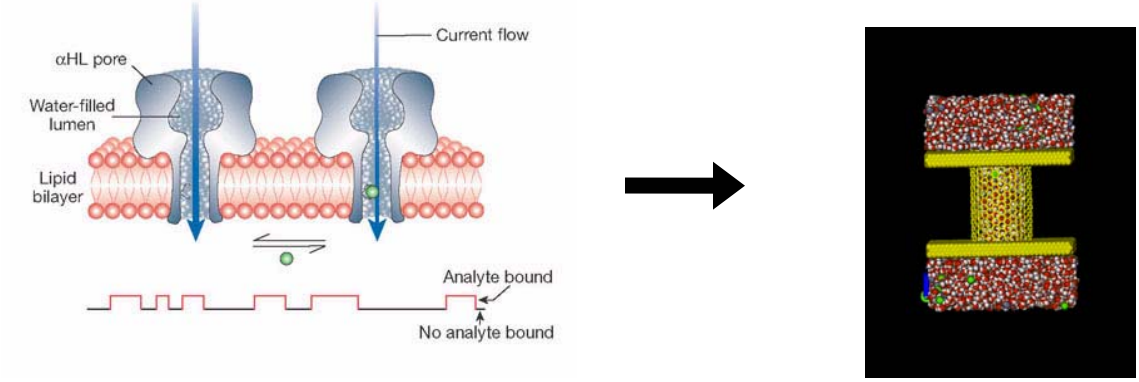

Figure 12. (Left) Schematic of single molecule detection by a modified alpha-Hemolysin channel: Current flow decreases on analyte binding. (Right) A design model of a functionalized carbon nanotube in a slab surrounded by water molecules and K+ and Cl- ions.

A review of recent literature showed that promising options for such a device that could be practically realized were Gold nanotubule membranes, ion beam etched silicon nitride membranes or single carbon nanotubes. Carbon nanotubes being rigid and having exciting electrical and mechanical properties seem ideal for an integrated circuit chip design but fundamental questions have to be addressed regarding transport of water and

ions through it. Quantitative information on fundamental modes of mass transport and transport rates have been obtained through carbon nanotubes of diameters of about 150 nm. It has been showed by molecular dynamics simulations that water molecules enter nanotubes of as small as 8.4 A diameter even though carbon is hydrophobic.

This project has recently shown for the first time the possibility of transport of an electrolytic solution (KCL) through a carbon nanotube by molecular dynamics simulations [9]. A short 13.4 A long uncapped (16, 16) single-walled nanotube was solvated in a reservoir of 1.85 M KCl and simulated using GROMACS. It was observed that ion occupancy was very low and that ions do not diffuse spontaneously into the tube (Figure 13). To attract the ions into the tube, partial charges of +/-0.38 e were placed at atoms on the rim of the tube to create a dipole − the positive charges being on top rim and the negative charges on the bottom rim. The tube was then fixed in the center of a box of length 33A and an external electric field was applied along the axial direction to mimic the membrane potential. It is observed that the occupancy increases significantly (See Figure 14). Once partial charges were shown to increase occupancy, the next step was to replace them with functional groups.

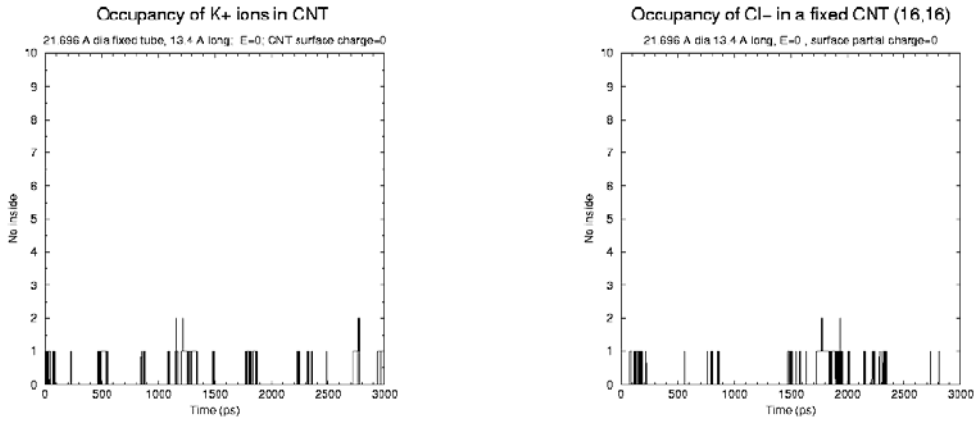

Figure 13. Ion occupancy in a (16,16) carbon nanotube (13.4 A L, 21.696 A dia) fixed in a solution of 1.85 M KCl. Ionis diffusion is very low without electric current or partial charges.

Functionalization of carbon nanotubes is a field of growing interest. Both side wall and end wall functionalization have been successfully realized in recent experiments. In simulations, an asymmetric functionalization of carboxylate and amino residues were used instead of the partial charges to mimic a real ion channel at either ends respectively. The partial charges were obtained from GROMOS force field database- carboxylate group from glutamate and amino group from lysine residues respectively. The functionalized carbon nanotube was then placed in a slab with similar properties of that of a lipid bilayer with a surrounding bath of 1.5 M KCL solution. An electric field of 0.15 V/nm was used to drive the ions through the tubes and the trajectories of K+ and Cl- ions are shown in Figure 15. The Chloride occupancy is much higher than potassium ion

occupancy even though the net partial charges at the mouths are same in magnitude. The attractive force between the COO- and the K+ ions is large that the K+ ions are "bound" to the COO- groups at the mouth reducing the K+ occupancy in the tube. Just like ionic channels, the functionalized carbon nanotube also seems to exhibit selective permeability of anions over cations. Further investigation is needed to explain the phenomena and how it can be utilized to control the rate and direction of ionic current.

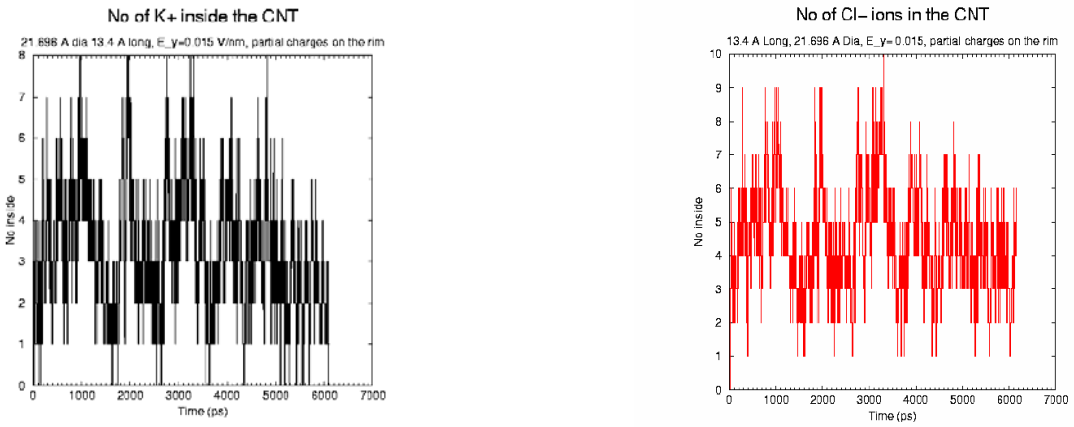

Figure 14. Ion occupancy in a (16,16) carbon nanotube (13.4 A L, 21.696 A dia) fixed in a solution of 1.85 M KCl with external electric field E=0.015 V/nm and partial charges of +/- 0.38 e on the rim atoms (positive on the top) and negative on the bottom.

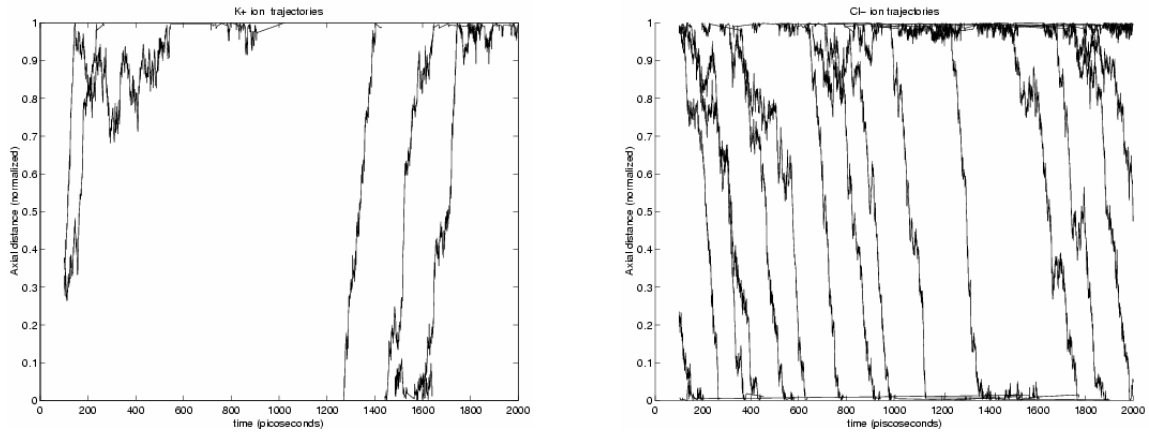

Figure 15. Motions z(t) of individual ions (K+ on the left and Cl- on the right) shown inside the nanotube along the nanotube axis. The rate of chloride ion passage is higher than the K+ ion passage indicating a selectivity of anions over cations.

8 QUANTUM CORRECTION TO VAN DER WAALS INTERACTIONS

Molecular Dynamics simulations give good results only to the accuracy with which the interatomic interaction potentials are correct[11]. Since at molecular scale, quantum effects also might be important along with classical forces, corrections have to be made to the various interatomic forces. In this section, we present a quantum correction to the van der Waals interactions which can be used to model nanoscale devices.

Many-body corrections to van der Waals interactions from semiclassical Casimir forces were calculated [10]. A basic analysis of the role of van der Waals terms in electromechanical systems was explored and its significance at the sub-nanometer scale demonstrated [13]. A recent theory of van der Waals interaction for shells of pure carbon is based on universal principles formulated in 1930's. A new approach is based on the quantum electrodynamical description of the van der Waals/Casimir forces[12]. A simple and effective model was developed to estimate the many-body contribution due to collective modes (plasmons). This contribution is believed to be a major portion of the total van der Waals energy because of the high oscillator strength of the plasmons. The theory reveals many-body terms that are specific for various low-dimensional graphite nanostructures and are not taken into account by standard one-body calculations within the dispersionless model by Lennard-Jones. We have demonstrated the use of the model for several systems (shown in Fig. 16): a double-wall nanotube (A), a nanotube on the surface (B) and a pair of single wall tubes (C). A significant difference has been shown for the dependence of the van der Waals energy on distance (Fig. 17), which is a consequence of quantum correction that was used.

The frequencies of the plasmons, which are mixed by the Coulomb interaction, are explicitly calculated . As a result of the mixing, the total system energy is lowered by the van der Waals contribution. The distance dependence of the new many-body correction term has a fractional exponent 5/2 for the tube-metal cohesion and 7/2 for tube-tube interaction. This is unlike an one-body energy given by LJ (6-12) potential. It was

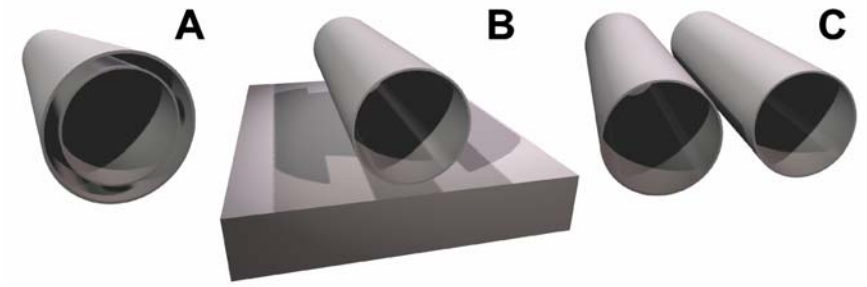

Figure 16. Geometry of nanotube systems for which a quantum correction to van der Waals forces has been calculated: (A) Double-wall nanotube, (B) single wall nanotube on a surface and (C) two single wall nanotubes.

known that the direct summation of atom-atom interactions for carbon nanotubes gives the exponents of 4 and 3 for inter-tube and tube-substrate cohesion, respectively. Thus, the quantum correction term is a totally new contribution and has to be taken into account along with the classical term.

Our model can be applied to simulations of biological channels, which have similar one-dimensional geometry. This allows one to calculate the van der Waals interactions more accurately which in turn would give better estimates parameters like diffusion coefficients. This will be done in the future.

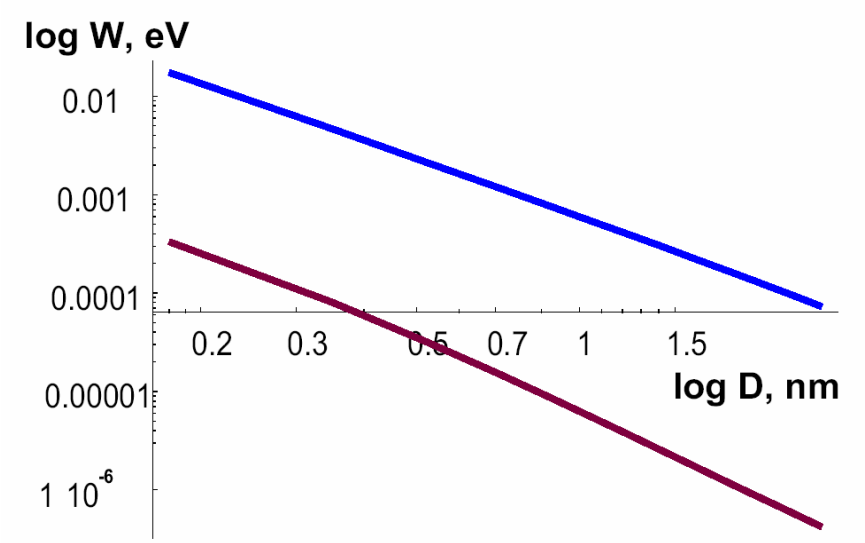

Figure 17. Van der Waals potential for SWNT on a metal substrate (upper) and between two identical tubes. Nanotube radius was 0.7 nm in the calculations.

9 CONCLUSIONS

Numerical and experimental investigations have been performed to understand and characterize properties of ion channels in order to use them as biosensors. This project was able to:

- Demonstrate use of mean field theories to predict selectivity and sensitivity based on continuum equations.
- Demonstrate multi-scale simulations that predict selectivity, sensitivity, and gating based on Langevin-Poisson simulations.
- Perform experiments showing how well porin and its mutants are described by continuum theories and by multi-scale simulations.
- Show biosensor activity of porin in experiments.
- Demonstrate carbon nanotubes can be used to mimic ion channels.
- Develop quantum correction to classical theories to calculate van der Waals forces.

The results obtained through this report have led to breakthrough advances in ion channels. Specifically, the drawbacks of continuum theory have been pointed out. Multiscale methods were developed to overcome these drawbacks. This approach is the key to analyzing the conductance, selectivity and sensitivity functions of ion channels. The multiscale methods can be used reliably to predict conduction through a variety of ion channels. Finally, the development of nanopore sensors has led to revolutionary ideas for detection of single molecules. The results obtained can be used in developing engineered ion channels or artificial ion channel like nano-devices in single molecule detection.

REFERENCES

[1] T. A. van der Straaten, R. S. Eisenberg, J. M. Tang, U. Ravaioli and N. Aluru, "Three-dimensional Poisson-Nernst-Planck Simulation of OmpF Porin", Biophysical Journal, 2001 80 (1) p. 115a. (abstract from 45th Annual Meeting of the Biophysical Society, Boston, MA, Feb 17-21, 2001)

[2] T. A. van der Straaten, J. M. Tang, R. S. Eisenberg, U. Ravaioli and N. Aluru, "Three-dimensional Continuum Simulations of Biological Ion Channels", in Technical Proceedings of the 2001 International Conference on Computational Nanoscience, Hilton Head, SC, Mar 19-21, 2001, pp. 39-42.

[3] T. A. van der Straaten, J. M. Tang, R. S. Eisenberg, U. Ravaioli and N. Aluru, "Three-dimensional Continuum Simulations of Ion Transport Through Biological Ion Channels: Effect of Charge Distribution in the Constriction Region of Porin", Journal of Computational Electronics, 2002, in press. (proceedings of the 8th International Workshop on Computational Electronics, Urbana, IL, Oct 15-17, 2001)

[4] T. A. van der Straaten, J. M. Tang, R. S. Eisenberg, U. Ravaioli, N. Aluru, S. Varma and E. Jakobsson, "A Study of Mutations of OmpF Porin Using Poisson-Nernst-Planck Theory", Biophysical Journal, 2002 82 (1) p. 207a. (abstract from 46th Annual Meeting of the Biophysical Society, San Francisco, CA, Feb 23-27, 2002)

[5] S. W. Chiu, S. Varma, E. Jakobsson, J. M. Tang, T. A. van der Straaten, R. S. Eisenberg, "Molecular Dynamics of Permeation in Porin and it's Mutant G119D", Biophysical Journal, 2002 82 (1) p. 208a. (abstract from 46th Annual Meeting of the Biophysical Society, San Francisco, CA, Feb 23-27, 2002)

[6] E. Jakobsson, S. W. Chiu, R. J. Mashl, S. Natarajan, Y. Tang, T. A. van der Straaten, S. Varma, "From Ion Channel Sequence to Physiology: Possibilities, Pitfalls and Realities", Biophysical Journal, 2002 82 (1) p. 340a.(abstract from 46th Annual Meeting of the Biophysical Society, San Francisco, CA, Feb 23-27, 2002)

[7] T. A. van der Straaten, S. Varma, S. W. Chiu, J. M. Tang, N. Aluru, R. S. Eisenberg, U. Ravaioli and E. Jakobsson, "Combining Computational Chemistry and Computational Electronics to Understand Protein Ion Channels", in Technical Proceedings of the 2002 International Conference on Computational Nanoscience, San Juan, Puerto Rico, Apr 21-25, 2002, pp. 60-63.

[8] T. A. van der Straaten, J. M. Tang, U. Ravaioli, R. S. Eisenberg, and N Aluru, "Simulating Ion Permeation Through the OmpF Porin Ion channel Using Three-

Dimensional Drift-Diffusion Theory", submitted to Journal of Computational Electronics.

[9] S. Joseph, R. J. Mashl, E. Jakobsson and N Aluru, "Ion channel based nanopore sensors: transport of electrolytes through carbon nanotubes", submitted to Technical Proceedings of the 2002 International Conference on Computational Nanoscience, Apr 2003.

[10] Rotkin, S. V. & Hess, K. (accepted to Int. J. Comp. Electronics) (2002).

[11] Dequesnes, M., Rotkin, S. V. & Aluru, N. R. Nanotechnology 13, 120-131. (2002)

[12] Girifalco, L. A., Hodak, M. & Lee, R. S. Physical Review B-Condensed Matter 62, 13104-10. (2000)

[13] Lennard-Jones, J. E. Proc. Roy. Soc London, Ser.A 129, 598-615. (1930)

[14] Hollerbach, U., Chen, D.P., and Eisenberg B.,Two and Three Dimensional Poisson-Nernst-Planck Simulations of Current Through Gramicidin-A. J. Scientific Computing 16 (4) 373-409 (2001)

[15] Gillespie, D. and Eisenberg, R.S. Modified Donnan potentials for ion transport through biological ion channels. Phys Rev E, 63 061902 1-8. (2001)

[16] Nonner, W., Gillespie, D., Henderson, D., and Eisenberg, Bob. (2001) Ion accumulation in a biological calcium channel: effects of solvent and confining pressure. J Physical Chemistry B 105: 6427-6436

[17] Schuss, Zeev, Nadler, Boaz, and Eisenberg, R.S. Derivation of PNP Equations in Bath and Channel from a Molecular Model, Phys Rev E 64: 036116 1-14, 2001.

[18] Gardner, Carl L., Jerome, Joseph W., and Eisenberg. R.S, Electrodiffusion Model Simulation of Rectangular Current Pulses in a Voltage Biased Biological Channel. (J Theoretical Biology, in the press) (2001)

[19] Mashl, R. J., Tang, Y., Schnitzer, J. and E. Jakobsson. Hierarchical approach to predicting permeation in ion channels. Biophys. J. 81: 2473-2483, 2001

[20] Nadler, B., Naeh, T., and Schuss Z. The stationary arrival of independent diffusers from a continuum to an absorbing boundary is Poisson. SIAM J. Appl. Math 62 (2) p. 433-447(2001)

[21] Gillespie, Dirk, and Eisenberg, Robert S. Physical descriptions of experimental selectivity measurements in ion channels. European Biophysics Journal (in the press). (2002).

[22] Gillespie, Dirk, Nonner, W., and Eisenberg, Robert S. Coupling Poisson-Nernst-Planck and Density Functional Theory to Calculate Ion Flux. Journal of Physics (Condensed Matter) In the Press (2002)

[23] Eisenberg, Bob Proteins, Channels, and Crowded Ions Biophysical Chemistry (in the press) (2002)

[24] Varma, S., Jakobsson, E., Ionization states of residues in OmpF and mutants-Effect of protein dielectric constant and ionic strength, in preparation.

APPENDIX A
Hierarchical Approach to Predicting Permeation in Ion Channels

Hierarchical Approach to Predicting Permeation in Ion Channels

R. Jay Mashl,*† Yuzhou Tang,‡ Jim Schnitzer,§ and Eric Jakobsson*†‡¶‖**

*Beckman Institute for Advanced Science and Technology, †Department of Molecular and Integrative Physiology, ‡Center for Biophysics and Computational Biology, §Department of Chemistry, ¶National Center for Supercomputing Applications, ‖Department of Biochemistry, **Bioengineering Program, University of Illinois, Urbana-Champaign, Urbana, Illinois 61801 USA

ABSTRACT A hierarchical computational strategy combining molecular modeling, electrostatics calculations, molecular dynamics, and Brownian dynamics simulations is developed and implemented to compute electrophysiologically measurable properties of the KcsA potassium channel. Models for a series of channels with different pore sizes are developed from the known x-ray structure, using insights into the gating conformational changes as suggested by a variety of published experiments. Information on the pH dependence of the channel gating is incorporated into the calculation of potential profiles for K^+ ions inside the channel, which are then combined with K^+ ion mobilities inside the channel, as computed by molecular dynamics simulations, to provide inputs into Brownian dynamics simulations for computing ion fluxes. The open model structure has a conductance of ~110 pS under symmetric 250 mM K^+ conditions, in reasonable agreement with experiments for the largest conducting substate. The dimensions of this channel are consistent with electrophysiologically determined size dependence of quaternary ammonium ion blocking from the intracellular end of this channel as well as with direct structural evidence that tetrabutylammonium ions can enter into the interior cavity of the channel. Realistic values of Ussing flux ratio exponents, distribution of ions within the channel, and shapes of the current-voltage and current-concentration curves are obtained. The Brownian dynamics calculations suggest passage of ions through the selectivity filter proceeds by a "knock-off" mechanism involving three ions, as has been previously inferred from functional and structural studies of barium ion blocking. These results suggest that the present calculations capture the essential nature of K^+ ion permeation in the KcsA channel and provide a proof-of-concept for the integrated microscopic/mesoscopic multitiered approach for predicting ion channel function from structure, which can be applied to other channel structures.

INTRODUCTION

The bacterial potassium channel KcsA marks the first permeation pathway high-resolution structure (Doyle et al., 1998) from the superfamily of the voltage-gated ion channels, which may be present in most living cells and underlie innumerable excitability, transport, signaling, and osmoregulatory functions (Hille, 1992). The primary open-closed gating of KcsA is by pH lowering (Heginbotham et al., 1999) with a voltage-dependent distribution of conducting open substates (Meuser et al., 1999). Perozo et al. (1999) used electron paramagnetic resonance spectroscopy (EPR) with site-directed spin labeling to show that during gating the transmembrane helix, which forms the lumenal surface of the pore, undergoes a rotational motion that provides a wider opening at the intracellular end of the channel.

A number of computational studies using methods of molecular dynamics (MD) (Allen et al., 1999, 2000; Åqvist and Luzhkov, 2000; Bernèche and Roux, 2000; Shrivastava et al., 2000; Shrivastava and Sansom, 2000), Brownian dynamics (BD) (Chung et al., 1999; Corry et al., 2000), and electrostatics methodologies (Roux and MacKinnon, 1999; Guidoni et al., 2000) have been done on KcsA, providing valuable information about the biophysics of the channel. General features of permeation as shown by these studies include the stabilization of the selectivity filter by ion occupancy, the obligatory single filing of ions through the selectivity filter, and the preferential attraction of cations into the selectivity filter by a combination of side chain and backbone charges exposed to the lumen. It has also been calculated that ions are significantly attracted into the wide cavity in the center of the channel by the dipole of the pore helix (Roux and MacKinnon, 1999).

However there has not yet been a quantitatively successful description of ion permeation in this channel that predicts electrophysiological properties by applying physics with no arbitrary parameters directly to experimentally measured structural data. The purpose of the present study is to describe the implementation of a hierarchical strategy (Jakobbson, 1998) combining multiple computational methods in a coordinated way in which all the parameters in the calculations are derived directly from structural data with no arbitrarily adjustable parameters and to apply this strategy to the KcsA potassium channel. As a high-resolution open KcsA channel structure is not yet available, we have constructed a series of structures of different opened sizes based on our best interpretation of published experimental data for how the open channel varies from the x-ray structural model, which is functionally closed. The resulting computed ion fluxes accurately reproduce known electrophysiologically measurable properties for this channel.

Received for publication 13 December 2000 and in final form 12 July 2001.

Address reprint requests to Dr. R. J. Mashl, University of Illinois, NCSA/Beckman Institute, 405 N. Matthews Avenue, Urbana, IL 61801. Tel.: 217-244-5818; Fax: 217-244-2909; E-mail: mashl@ncsa.uiuc.edu.

0006-3495/01/11/2473/11 $2.00

MATERIALS AND METHODS

Molecular modeling of the open channel

Our strategy for molecular modeling of the channel takes several factors into account. 1) A motion of the M1 transmembrane helix and pore-lining M2 transmembrane helix tending to open the intracellular end of the channel, as suggested by the EPR spectroscopy of Perozo et al. (1999). 2) A degree of opening of the intracellular end of the channel sufficient to permit tetrabutylammonium ion (TBA) to be an optimal channel blocker relative to other quaternary amines (Meuser et al., 1999; Splitt et al., 2000) and to enter the channel completely into the deep cavity (Zhou et al., 2001). 3) The preservation of the shape of the extracellular vestibule, as suggested by experimental data, that differences in toxin binding affinity of open and closed K channels is a function of interactions among K ions in the channel rather than a change in the shape of the vestibule (Terlau et al., 1999). 4) The maintenance of hydrophobic matching of the transmembrane helices with the surrounding implicit membrane, by maintaining a constant helix tilt with respect to the bilayer normal, which is the same as the channel axis. The tendency to preserve hydrophobic matching is a generally accepted principle of protein-lipid interactions, albeit not always perfectly obeyed (Killian, 1998). The specific modeling process is described below.

The x-ray structure of KcsA in the Protein Data Bank is an L90C mutant with missing residues 1 through 22 and 120 through 158 and truncated side chains at Arg-27, Ile-60, Arg-64, Glu-71, and Arg-117 (Doyle et al., 1998). This structure was refined by completing the truncated side chains and optimizing their positions using the program Modeler (Sali et al., 1990). The ends of the four subunits were capped with the nontitratable groups CH_3—C═O and NH—CH_3 as extensions of the α-helices. A series of energy minimizations was done using a distance-dependent dielectric, leading to a structure that satisfied the structural criteria of Procheck (Laskowski et al., 1993) and information-based probability density functions (Wall et al., 1999).

To achieve an opening of the intracellular end of the channel consistent with the hydrophobic matching and maintenance of the external vestibule shape, the extracellular ends of the transmembrane helices M1 and M2 were kept fixed, and the M2 helices were rotated about an axis parallel to the membrane normal (channel axis). The M1 helices were rotated in the same fashion as necessary to eliminate steric overlap with M2. The M1 was rotated approximately the same amount as was the M2.

The refined crystal structure and a structure formed by a 20° rotation of the M2 were inspected for gaps in packing as visualized by RasMol (Sayle and Milner-White, 1995) in space-filling mode, as seen in Fig. 1, *A–D*. When viewed from the extracellular end and from within the membrane plane, both the closed and opened structures have some gaps between the M1 and M2, which are presumably filled by hydrocarbon when the channel is in a membrane. Our construction procedure may widen existing gaps but introduces no substantial new gaps into the protein structure.

Fig. 1 *E* shows the diameter of the permeation pathway as determined by the program HOLE (Smart et al., 1993) and its variation along the axis in the Doyle et al. (1998) x-ray structure and in structures of various opened sizes. (For convenience, the term "opened channel" refers to the 20°-opened structure unless otherwise stated. The 20° estimate for the degree of rotation of the M2 helix in the fully opened channel is based on the estimate from Perozo et al., 1999.) Two very narrow regions in the x-ray structure are found at the selectivity filter and near the intracellular end of the channel. The intracellular end widens to an average diameter of ~13.5 Å in the opened channel. This size is consistent with experimental evidence on channel blocking by quaternary ammonium ions (Meuser et al., 1999; Splitt et al., 2000), which suggests the size of the intracellular opening for the maximally conducting substate of the channel is larger than TBA. Further evidence that the channel opens widely enough to permit TBA to enter comes from a recent x-ray structure of the channel-TBA complex showing that TBA enters completely into the channel (Zhou et al., 2001). (The K channel structure complexed with TBA is not much different from the closed structure, but a transient opening at the intracellular end would be required for the TBA to enter.) Estimates for the effective molecular diameter of TBA vary from a minimum of ~9.5 Å (Splitt et al., 2000) to a value of 11.6 Å based on an idealized geometry (Huang et al., 2000).

It should be noted that our open channel structure is not certain in complete detail. However, there is strong experimental evidence that the intracellular end of the channel opens to approximately the extent that we suggest, whereas the extracellular vestibule and selectivity filter do not change in dimension or conformation during channel opening. On the other hand, the M2 residues are generally farther away from the channel axis in our opened channels as compared with the closed channel, whereas EPR experiments (Perozo et al., 1999) suggest that some of the residues move closer to the axis. This might be achieved by adding to the motion that we have suggested a rotation of the helix about its axis and/or a kink within the helix itself. Given the absence of direct evidence for specific movements of these kinds and the subtleties inherent in interpretation of EPR data, we judged it not useful to pursue further structural modeling without more detailed structural data on the open state. Because of the residual uncertainty of the structure, as well as other approximations in the calculations that we discuss later in the paper, we emphasize that our results should be considered as only semiquantitative representations of the channel behavior. We believe the major conclusions of the paper depend only on the intracellular end of the channel opening to approximately the same degree as in our model with the selectivity filter unchanged and will therefore stand as long as the correct model of the open channel has these features.

Electrostatics: pK_a calculations and potential profile for ion permeation

Electrostatics calculations were used to calculate the ionization states of protein residues under various physiological conditions. We used the method described in Gilson (1993) and Antosiewicz et al. (1994) as implemented in the University of Houston Brownian Dynamics (UHBD) suite of programs (Madura et al., 1995) used to calculate electrostatic energies. UHBD requires the specification of dielectric constants for the protein and surrounding electrolyte. To emulate the low-dielectric environment around the channels for these calculations, a layer (thickness, 23.4 Å) of neutral nonpolar spheres (radius, 2.0 Å), postulated to be situated in between the aromatic residues at the lipid-water interfaces (Cowan et al., 1992), was placed around each structure, as shown in Fig. 1 *F*. The spheres were packed at hydrocarbon densities out to ~37 Å from the channel axis. The protein dielectric constant was set to 20, which appears to be the optimum for computing the ionization states of residues in many proteins (Antosiewicz et al., 1994), and the nonpolar spheres were assigned a value of 20 as well. Outside the regions delineated by protein and membrane the dielectric constant was set to 80 to represent water. UHBD automatically accounts for the image charges arising from introduction of a dielectric interface.

The partial charge parameters used in the calculation of electrostatic energies were taken from the CHARMm (Brooks et al., 1983) parameter set and radii from the OPLS (optimized parameters for liquid systems) parameter set (Jorgensen and Tirado-Rives, 1988), following Antosiewicz et al. (1994). Reference pK_a values corresponding to the pK_a values of model compounds in solution for each titrating residue type are taken from Antosiewicz et al. (1994). A modified approach (Tanford and Roxby, 1972) was used to determine effective pK_a values in which an ionization polynomial is evaluated exactly for clusters of residues with significant charge-charge correlations and a mean field approximation is used for less significant intercluster interactions (Gibas et al., 1997). The cluster method requires that each histidine be assigned a tautomer, and in all cases the tautomer in which Nϵ2 is the titrating site was used. The calculations used a finite-difference method for computing electrostatic potentials at the lattice points of a grid of spacing 1.2 Å surrounding the titratable site. Focusing grids of sizes 1.0, 0.75, and 0.25 Å were used to refine the potentials. (The position and orientation of the lattices were fixed with

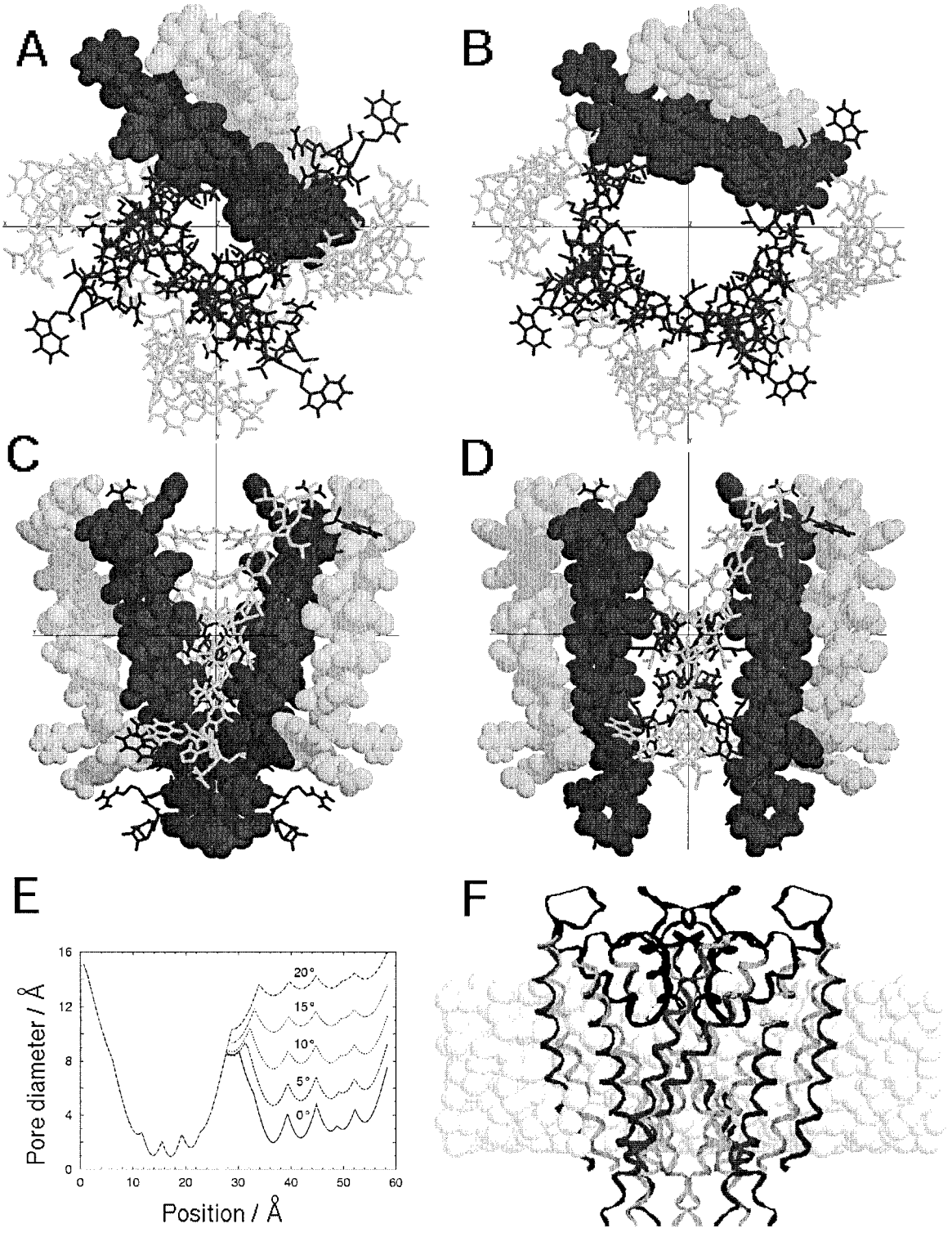

FIGURE 1 Packing of transmembrane helices in the closed (*A* and *C*) and modeled 20°-opened (*B* and *D*) KcsA structures (M2 helices, *dark gray*; M1 helices, *light gray*). The P regions of the channel are omitted for clarity. Views in *A* and *B* are from the extracellular end of the channel. Views in *C* and *D* are side-on from the membrane plane such that the interhelical gaps appeared to be maximized. (*E*) Channel pore diameter given by the protein van der Waals surface versus position along the channel axis, as measured by the program HOLE (Smart et al., 1993), for several M2 helix rotations (x-ray model, 0°). The protein extends from 0–60 Å with the extracellular end oriented at left. The narrow region from ~10–25 Å contains the selectivity filter, and the narrow region from ~30–50 Å in the x-ray structure is lined with aliphatic side chains from the four M2 helices. (*F*) Superimposed ribbon representations of the channel in the closed (*gray*) and 20°-open conformation (*dark gray*) as viewed from the membrane plane (*spheres, light gray*) for electrostatics calculations. The remaining sections corresponding to the selectivity filter, extended, and turret regions (*black*) are common to both structures. Orientations in panels *C*, *D*, and *F* are with the extracellular end at top.

respect to the coordinate axes for all channels studied.) The pK_a values were computed using the linear Poisson-Boltzmann electrostatics module within UHBD. Test calculations with the nonlinear Poisson-Boltzmann method revealed that the modifications of the ionization states were not large enough to justify their greater computational demand. The ionization states were not substantially affected by either the presence of a single on-axis K^+ ion or by ionic strength in the range 0.15 to 1.50 M. Symmetric pH conditions were used, and all calculations were carried out at 298 K.

For computing potential profiles of a single ion along the channel axis, the calculated ionization states were converted into new, effective partial charges for the side chain atoms. The total force acting on the ion as a function of position along the axis was then calculated using UHBD. The axial component of this force was integrated over the length of the channel to give the potential profile of the ion. Because of the asymmetry of charge in the channel protein combined with the absence of shielding charges in the electrolyte in this reduced system, it was necessary to normalize the computed transmembrane potential to zero by the addition of a constant field.

Molecular dynamics: determining the mobility of ions within the channel

MD simulations of ion motions throughout the channel were performed using the program GROMOS96 (van Gunsteren et al., 1996) with solvation of the refined version of the channel by methods we previously used for the gramicidin channel (Chiu et al., 1993) and for part of the permeation pathway for a model of the sodium channel (Singh et al., 1996). Specifically, the wide parts of the channel pore were hydrated, and the ends of the channel were bathed in approximately hemispherical caps of water extending to the aromatic collars. Three potassium ions, two of which were initially located in the outer crystallographic positions at either end of the selectivity filter and one ion located in the central cavity, were included for equilibration for 1 ns at 298 K. To prepare the system for ion diffusion measurements, two of the ions were replaced with water molecules, and the system was re-equilibrated while strongly restraining the restraining ion to the channel axis. The position of the strong restraints was updated in 1-Å increments along the channel axis, allowing for reequilibration in each instance. Several reequilibrated systems were selected to represent a subset of ion positions along the channel axis, including those in which the ion was located in the outer vestibule, within the selectivity filter, in the central cavity, and in the narrow, hydrophobic part of the channel. Production runs of 27 ps with no restraints on the ion were generated in each region of the channel.

Velocity autocorrelation functions were calculated for the unrestrained ion trajectories in each part of the channel. The velocity autocorrelation function (McQuarrie, 1976) relevant to one-dimensional motion of ions along the channel axis (see below) is given by the expression $\langle v_z(t_1)v_z(t_2)\rangle$, in which v_z is the z-component of the velocity of the ion at two times, t_1 and t_2, and the angle brackets denote an equilibrium average. In an equilibrium system the correlations depend on only differences in time $t = t_2 - t_1$. We fit the velocity autocorrelation function to the single exponential function

$$\langle v_z(0)v_z(t)\rangle = A_0[v(0)]^2\exp(-t/\tau), \qquad (1)$$

in which A_0 is a scaling factor and the time constant, τ, is related to the fluid dynamic diffusion coefficient, D_f, by the expression

$$\tau = mD_f/k_BT \qquad (2)$$

in which m is the mass of the ion, T is the temperature, and k_B is Boltzmann's constant.

TABLE 1 Input parameters for the Brownian dynamics simulation program for the fully opened channel

Parameter	Value
Channel length	6.0 nm
Channel mouth diameter (open channel)	1.35 nm
Dielectric constant for ion-ion interactions	20
Channel diffusion coefficient	2.51×10^{-5} cm^2 s^{-1}
Bath diffusion coefficient	2.51×10^{-5} cm^2 s^{-1}
Size of time step	0.4 ps
Length of each simulation	0.2 ms

Brownian dynamics: calculating fluxes and distributions within the channel

BD simulations were performed using methods we have previously reported (Cooper et al., 1985; Bek and Jakobsson, 1994) to compute ion fluxes. These calculations are one-dimensional, in effect constraining the ions to move along the channel axis. For each time step, each ion in the system is moved a certain distance based on a combination of deterministic motion due to a free energy gradient and random motion representing thermal fluctuations, according to the equation

$$\Delta z = -\frac{D}{RT}\left(\frac{\partial U}{\partial z}\right)\Delta t + \xi(2D\Delta t)^{1/2}, \qquad (3)$$

in which Δz is the distance that an ion moves in the time interval Δt, D is the ion diffusion coefficient, R is the ideal gas constant, T is the absolute temperature, $\partial U/\partial z$ is the free energy gradient, and ξ is a random number chosen from a normal Gaussian distribution centered at zero. The free energy gradient, $\partial U/\partial z$, is approximated by its electrostatic component $z_{ion}F(\partial V/\partial z)$, in which z_{ion} is the valence of the ion, F is Faraday's constant, and $\partial V/\partial z$ is the voltage gradient. The voltage gradient is the force seen by an ion due to the channel and surrounding solvent as it moves through the channel, plus the applied transmembrane voltage, plus the electric field due to other ions in the channel.

A summary of the parameters for the BD calculations is listed in Table 1. Based on the MD results (described in the Results section below), we set the K^+ diffusion coefficient inside and outside the channel equal to the dynamic ion diffusion coefficient for K^+ in bulk water. A dielectric constant of 20 was used for ion-ion interactions, which is consistent with the ions being in a narrow cavity surrounded by protein. The time step was 0.4 ps, and the time step and mobility together lead to a mean thermal jump distance of 0.45 Å per time step. Ions enter the channel by means of the "entrance tube" algorithm (Cooper et al., 1985; Jakobsson and Chiu, 1987; Bek and Jakobsson, 1994), a particular implementation of the flux-over-population method (Farkas, 1927, as cited by Hänggi et al., 1990). The capture radius for ions attempting to enter the channel was taken as the average radius of the intracellular half of the channel (Fig. 1*E*). Thus the BD simulations contain no arbitrarily chosen parameters.

RESULTS AND DISCUSSION

Computing potential profiles

An overview of our open channel models is shown in Fig. 1, *A–F*. Detailed information about the generation of these structures is given in the Materials and Methods section. Given these models, we first compute the ionization states of the titratable residues in both the x-ray and opened channel structures at pH 4 and 7, as it has been demon-

TABLE 2 Comparison of ionization states of titratable side chains

	pH 7		pH 4		
Residue	0°	20°	0°	20°	GROMOS96
His-25	0.043	0.021	0.922	0.931	0
Arg-27	1.000	1.000	1.000	1.000	1
Tyr-45	0.000	−0.001	0.000	0.000	0
Glu-51	−0.998	−0.997	−0.598	−0.486	−1
Arg-52	1.000	1.000	1.000	1.000	1
Tyr-62	−0.003	−0.003	0.000	0.000	0
Arg-64	1.000	1.000	1.000	1.000	1
Glu-71	−0.486	−0.513	−0.017	−0.020	−1
Tyr-78	0.000	0.000	0.000	0.000	0
Asp-80	−0.999	−0.999	−0.973	−0.974	−1
Tyr-82	0.000	0.000	0.000	0.000	0
Arg-89	1.000	1.000	1.000	1.000	1
Cys-90	−0.001	−0.002	0.000	0.000	0
Arg-117	1.000	1.000	1.000	1.000	1
Glu-118	−0.963	−0.997	−0.315	−0.354	−1

The values (in units of *e*) were averaged over the four subunits. The data are for the x-ray (0°) and opened channel structures (20°) embedded in a dielectric slab and exposed to electrolyte (ionic strength, 200 mM). Also shown are the standard partial charges used in the molecular dynamics simulations for the x-ray structure at neutral pH.

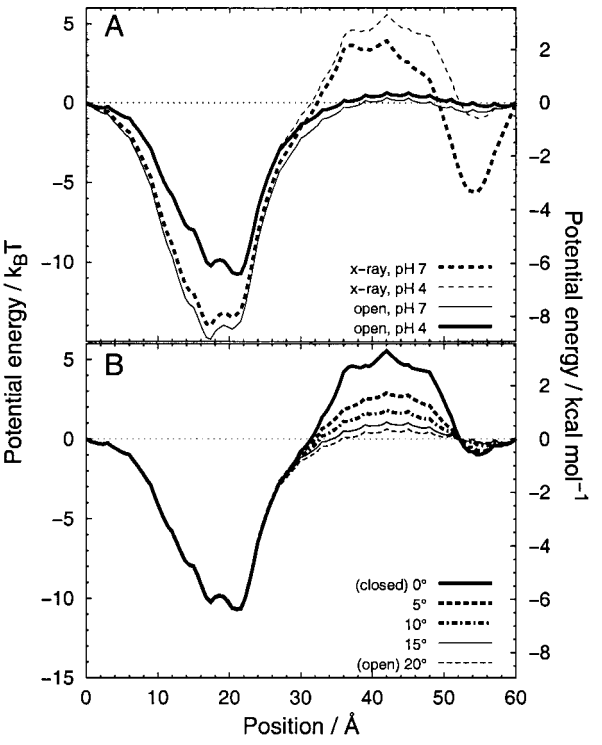

FIGURE 2 (*A*) Potential profile of a potassium ion in translocating the channel along the channel's axis in the x-ray and open channel structures at neutral and acidic pH using partial charge data from Table 2. Those profiles in bold relief correspond to physiologically relevant conditions and are the basis for the subsequent calculations. (*B*) Potential profiles for K^+ in the structures of intermediate open sizes (as measured by the degree of M2 rotation) at pH 4. Note the decline in the Born energy barrier near the intracellular end of the channel as the channel is opened.

strated experimentally that the channel is functionally closed at pH 7 and is fully open at pH 4 (Cuello et al., 1998; Heginbotham et al., 1999). The results in Table 2 show that the glutamates, located in the vestibule and toward the C terminus, undergo partial protonation at low pH, whereas the histidines, toward the N terminus, carry a full charge. (For comparison, the values used by the GROMOS96 simulation package standard force field are also given and are in close correspondence with the computed ionization states at neutral pH for all residues except for Glu-71.) Ionization states of side chains at various ionic strengths were computed similarly. We found that neither the channel conformation nor variation of the ionic strength had an appreciable effect on computed ionization states.

Fig. 2 shows the potential profiles as seen by a K^+ ion traversing the channel along the channels axis. The potential profile for the x-ray conformation at pH 7 has three notable features: a deep potential well containing the selectivity filter, a second potential well near the intracellular end of the channel, and a pronounced potential barrier in the narrow region of the channel. All curves show a deep potential well near the extracellular end of the channel that is due to the negatively charged carbonyl oxygens in the selectivity filter and, to a lesser extent, to the negatively charged residues in the vestibule of the channel. This well is somewhat shallower at pH 4 than at pH 7 due to the partial neutralization of Glu-51 in the vestibule. The potential well near the intracellular end of the x-ray structure is due to negatively charged Glu-118 and shows a large pH dependence. The pH dependence here for the open structure is much less because Glu-118 is now farther from the channel axis. The barrier, resulting from the dielectric contrast between the high-dielectric electrolyte and the low-dielectric protein and surrounding membrane, is an image potential barrier (Sancho et al., 1995) that can be thought of as a Born energy, or desolvation energy, associated with moving an ion from the surrounding electrolyte into the narrow nonpolar channel interior. The profile for the opened channel at pH 4 reveals that this image potential barrier is greatly reduced upon widening the channel lumen. It is seen that the depth of the potential well at the selectivity filter is not very sensitive to the degree to which the channel is opened but is sensitive to the ionization state of the protein. The potential profiles as computed for other ionic strengths (not shown) provide similar results. Fig. 2 *B* shows the potential profile for the potassium ion traversing the channel axis for different sizes of channel openings at pH 4. It is seen that the potential barrier near the intracellular end of the channel is systematically reduced as the channel is opened further.

In summary, our modeling and electrostatics calculations thus show that the depth of the potential well at the selectivity filter is controlled by the ionization states of titratable residues of the protein, whereas the image potential barrier

near the intracellular half of the channel is controlled by the size of the pore at the intracellular end.

Computing ion mobilities

Velocity autocorrelation functions were calculated from the ion trajectories generated by MD simulations. Values for the fluid dynamic diffusion coefficient (due to local friction), determined from Eqs. 1 and 2, were found to range from 1.8×10^{-5} to 3.3×10^{-5} cm^2 s^{-1}, in close agreement with the experimental value of 2.5×10^{-5} cm^2 s^{-1} that pertains to K^+ ions in bulk water (Hille, 1992). Because of the complexity of the ion solvation environment, the velocity autocorrelation functions were more complex than simple exponentials. However, the best fit to an exponential still suffices to give an approximately correct diffusion coefficient. In the wide part of the channel, the ion is in fact solvated by water. In the narrow part of the channel, it appears from our results that the carbonyl oxygens substitute approximately equivalently to bulk water oxygens in determining the local friction for ion movement. It should be pointed out that the diffusion coefficient in this case is not the effective diffusion coefficient, but rather the reciprocal of the local friction. The effective diffusion coefficient in the selectivity filter is certainly less than in bulk water, due to the potential well created by the carbonyl oxygens, even while the local friction is the same as bulk water. This situation is similar to that pertaining in gramicidin, where we earlier found that the local friction for sodium ions in gramicidin was similar to bulk water, whereas the effective diffusion coefficient was lower by a factor of 10, due to the potential wells created by carbonyl oxygens in that structure (Chiu et al., 1993).

Computing ionic fluxes

Ionic fluxes were calculated using a one-dimensional BD method for the ions. The resulting conductance calculated for the closed channel at both pH 7 and 4 was a fraction of a picosiemen. In Fig. 3 *A* the computed current-voltage (I–V) curve for the fully opened channel for 250 mM K^+ shows an approximately linear relationship over the voltage range of $\pm$100 mV in agreement with the experiment. The corresponding average channel conductance over this voltage range is ~110 pS, in reasonable agreement with experimentally determined maximal conductances of 90 pS (Schrempf et al., 1995) and 135 pS at 200 mM K^+ (Cuello et al., 1998) and of ~130 pS at 250 mM K^+ (Meuser et al., 1999). The mean number of ions in the channel and the Ussing flux ratio exponent were computed for various transmembrane voltages (Table 3) and were found to be close in value to each other, in agreement with the original theory relating these two quantities (Hodgkin and Keynes, 1955). Although there are currently no experimental flux ratio

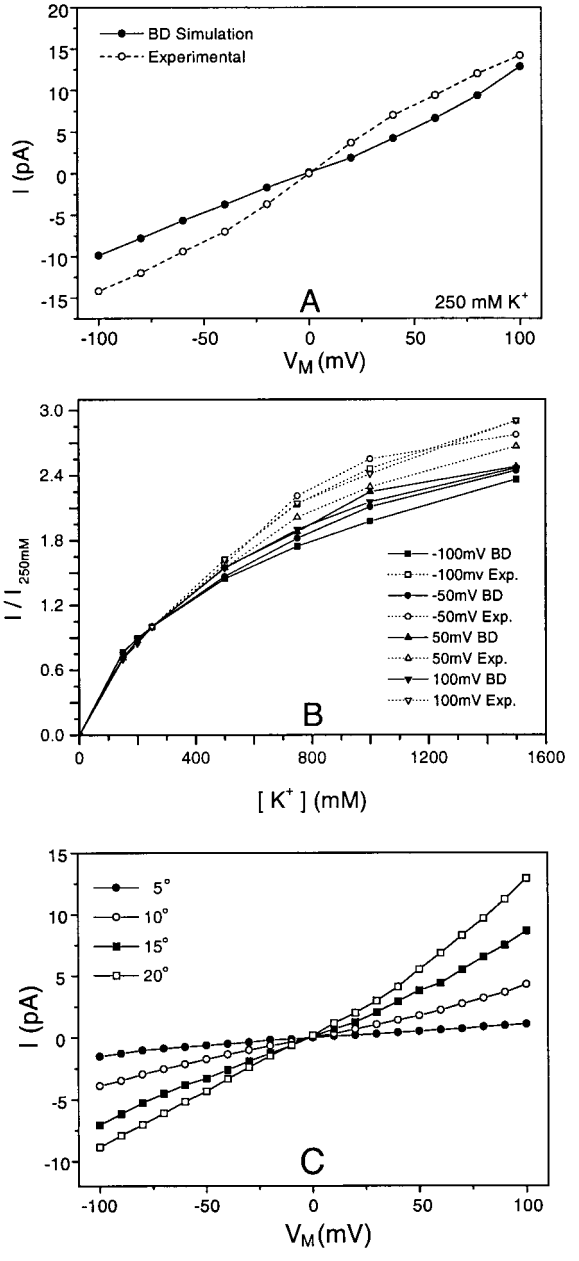

FIGURE 3 (*A*) Current-voltage curves as computed by BD for the opened channel at pH 4 for 250 mM K^+ using the parameters in Table 1, compared with experimental results (Meuser et al., 1999) for the largest conducting substate under comparable conditions. Each simulated point represents a 0.2-ms-long simulation. (*B*) Current-concentration curves for the opened state at pH 4 for several membrane potentials with parameters from Table 1, compared with experiment (Meuser et al., 1999). Each curve is normalized to the respective value of the current at 250 mM K^+. (*C*) Current-voltage curves as computed by BD for channels of different opened sizes at 250 mM K^+. Two factors are responsible for the difference in currents. One is the size of the Born potential barrier near the intracellular end of the channel, as shown in Fig. 2 *B*. The other is the capture diameter for ions to impinge on the intracellular end of the channel, as visualized in Fig. 1 *E*. The capture diameters used for the calculations shown were 5.5 Å for 5°, 8.4 Å for 10°, 11.0 Å for 15°, and 13.5 Å for 20°. In all calculations shown in Fig. 3 the standard deviations of the simulated currents are smaller than the size of the data symbols used.

TABLE 3 Mean number of ions in the channel and Ussing flux ratio exponent as a function of transmembrane voltage for the opened channel at pH 4 and at 250 mM K^+, as computed by Brownian dynamics

Voltage (mV)	Mean number	Ussing flux ratio exponent
100	2.01	2.08
80	2.01	2.22
60	2.02	2.16
40	2.02	2.25
20	2.03	2.14
0	2.02	Indeterminate
−20	2.03	2.00
−40	2.03	2.16
−60	2.03	2.21
−80	2.02	2.09
−100	2.01	2.01

exponent data for KcsA, a recent study (Stampe et al., 1998) on an inward-rectifying K channel has shown ratios between 2.1 and 2.5 for membrane potentials ranging from −50 to −25 mV, which is in close agreement with our simulations.

Fig. 3 *B* shows the relationship between current (normalized to the 250 mM K^+ value) and concentration for the opened channel at several transmembrane voltages with comparison with experimental values (Meuser et al., 1999). (The channel-ion potential profiles were recalculated for each ion concentration.) Whereas the calculated concentration dependence of the simulated current is similar to that seen in experiment, the simulated currents tend to saturate at a slightly lower concentrations. We believe this behavior may be due to the approximation of one-dimensional ion motion implicitly used in the BD simulations, an approximation that is not as good at near-saturating concentrations as it is at lower more physiological concentrations.

Fig. 3 *C* shows the I–V curves for single channels for the different open sizes shown in Fig. 1 *E*. The modeled partially opened channels produce intermediate conductances in a fashion similar to conducting substates. The conductance increase as the pore size increases is partly due to the reduction in the Born potential barrier near the intracellular end (Fig. 2 *B*) and partly due to the increase in the capture diameter of the channel when the channel opening is larger. It may be that the basis of conducting substates in K channels is the size of the pore aperture at the intracellular end of the channel in a similar fashion to this model.

Features of Brownian ion trajectories

The sample of BD ion trajectories in Fig. 4 demonstrates the extreme ability of the negative charges lining the selectivity filter to concentrate cations. Here the ribbon structure of the opened channel is superposed on the trajectories so that the structural basis for the preferred ionic positions can be seen. There is a clear preference for a double-occupancy state in the selectivity filter, consistent with the computed mean number of ions in the channel (Table 3). The histogram of ion positions computed for the entire length of the BD simulation reveals two prominent peaks in the selectivity filter separated by ~7 Å, similar to the pattern of ion distribution as revealed by x-ray crystallography (Doyle et al., 1998). Fig. 4 also shows the occasional appearance of a single-occupancy state in the selectivity filter where the mean position of the single ion lies in the carbonyl "cage" in between the two that are preferred during double occupancy. This relationship between singly and doubly occupied states is similar to the findings of recent free-energy perturbation MD simulations (Åqvist and Luzhkov, 2000).

The trajectories in Fig. 4 also reveal that two ions occupying the selectivity filter move nearly in unison in response to an incoming third ion. The movement of one ion out of one end of the selectivity filter and the entrance of another from the other end is so close to simultaneous that on the time scale of Fig. 4, the trajectories suggest a "knock-off" mechanism. Recent experimental data on channel blocking of KcsA by barium ions has suggested similarly that a third ion could enter the selectivity filter to push the queue of ions along (Jiang and MacKinnon, 2000).

Because the selectivity filter holds two ions practically all the time, and because the mean channel occupancy is only fractionally over two (Table 3), it follows that the wide part of the channel hardly ever holds more than one ion. This shows why the one-dimensional approximation to the motion is reasonably accurate. In the selectivity filter the motion really is one-dimensional because the channel is narrow there. In the wide part of the channel, only the projection of the motion of the single ion onto the channel axis is all that contributes to the flux. Thus, ignoring the lateral motion of the ions in this region does not introduce gross inaccuracies into the calculation.

Ion channels are essentially electrical resistance elements (Hodgkin and Huxley, 1952). In the KcsA (and presumably other) potassium channels, the selectivity filter is in series with the wider portions of the channel at the extracellular and intracellular ends. We analyzed this channel as two resistors in series, one comprising the selectivity filter and the other the rest of the channel. Because the selectivity filter is almost always doubly occupied, regardless of bath electrolyte concentration, we postulate that the resistance of the selectivity filter is a constant. We further postulate that the resistance of the rest of the channel is inversely proportional to electrolyte concentration, similar to bulk electrolyte. This leads to the functional form

$$R = R_f + A/[K^+], \tag{4}$$

in which R is the resistance of the single channel (reciprocal of the conductance), R_f is the intrinsic resistance of the selectivity filter, and A is a constant. This model of resistors in series provides a physical basis for the frequently ob-

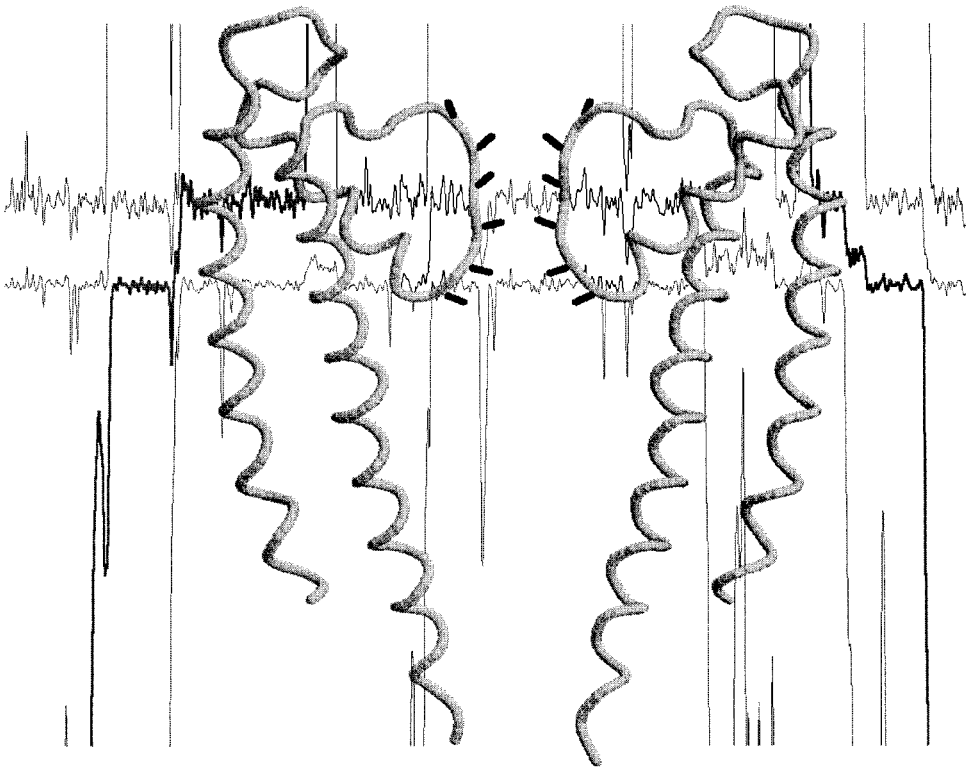

FIGURE 4 A 120-ns sample of BD ion trajectories in the opened channel at pH 4 at 0 mV membrane potential in 250 mM K^+ solution using parameters in Table 1. For ease of visualization the data were smoothed using a window of 120 ps, effectively filtering out oscillations greater than $\sim 10^{10}$ Hz. Ions that have successfully traversed the channel in this time window are shown in bold relief. A RasMol (Sayle and Milner-White, 1995) ribbon representation of the backbones (*gray*) from two opposing subunits showing the negatively charged carbonyl groups (*black*) projecting into the selectivity filter lumen is superposed.

served property of ion channels to follow Michaelis–Menten kinetics (Aidley and Stanfield, 1996). The solid and dashed lines in Fig. 5 show the fit of Eq. 4 to both computed and experimental data (same data as Fig. 3 *B*) for a voltage of 100 mV. It is seen that the fit is very good. Similarly good fits to Eq. 4 are obtained for the full range of simulated voltages. In this view, the reciprocal of R_f ($\sim$500 pS) is the theoretical maximal conductance achievable by a potassium channel if all resistance in series with the selectivity filter could be eliminated. The ratio of selectivity filter resistance to that of the wider pore regions was computed (Fig. 5, *inset*). At low bath potassium concentrations, the majority of the KcsA resistance appears to be in the wider regions of the channel, whereas at high concentrations the majority of the resistance is in the selectivity filter.

It may at first seem counterintuitive that at physiologically relevant ion concentrations the majority of the resistance is in the wide part of the channel. To understand this, consider that the conductance of any medium through which ions flow is a product of the mobility and the charge density. To some extent the effective mobility of the ions is reduced in the selectivity filter by the negative charges of the backbone carbonyl oxygens, yet the concentration is increased

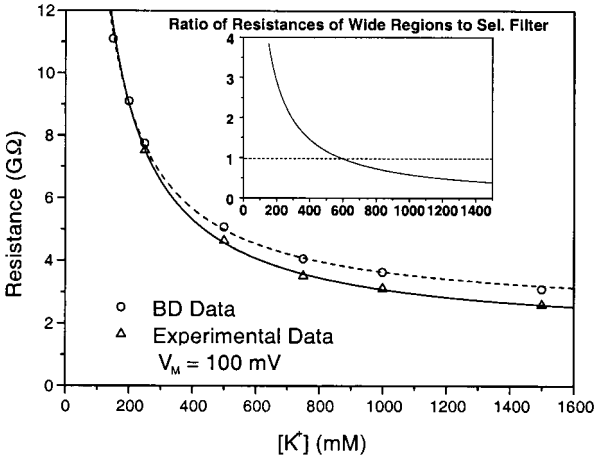

FIGURE 5 Opened-channel resistance, *R*, computed from the ratio of voltage to current, as a function of electrolyte concentration at 100 mV for BD simulations (*circles*) and for electrophysiological measurements of the maximal conducting substate (Fig. 4 of Meuser et al., 1999) (*triangles*). Fitting of the data sets to Eq. 4 yielded constants of $R_f = 2.3$ GΩ and $A = 1.34 \times 10^9$ Ω·M for the simulations and $R_f = 1.6$ GΩ and $A = 1.48 \times 10^9$ Ω·M for the experiments. The *inset* shows the ratio of the resistance of the wide regions of the channel to the resistance of the selectivity filter for the simulations.

enormously ($\sim$20 M K^+), which is more than compensating for the reduction in effective mobility.

SUMMARY AND CONCLUSIONS

We have described and carried out a hierarchical strategy for characterizing the permeation of the KcsA potassium channel. This strategy begins with the x-ray crystal structure of the channel (Doyle et al., 1998) from which a series of opened channel structures was built by a process of rotating the transmembrane helices surrounding the channel permeation pathway in a manner generally consistent with blocking experiments, toxin-binding studies, and hydrophobic matching principles. Experimental pH conditions for the functionally closed and open conformations were incorporated through pK_a calculations of the ionization states of the titratable residues. Electrostatics calculations were used to obtain the potential profiles of ions along the channel axis. MD simulations were performed to obtain the ion diffusion coefficient for incorporation into BD calculations for generating ion fluxes. Although the calculations have many approximations (e.g., representing the ion-channel potential profile by an electrostatic calculation, representing the ion motion through the channel as one-dimensional, representing ion-ion interaction in the channel as governed by an equivalent dielectric constant, not having a high-resolution structure for the open form of the channel), the calculations appear to capture the essence of the permeation through the KcsA channel, based on the close correspondence between the behavior of the real channel and the BD simulations.

Examination of the calculations suggests several features of K^+ permeation through potassium channels. 1) The x-ray model structure of the KcsA channel is closed not by physical occlusion but rather by image forces that arise in attempting to move an ion from the electrolyte to a narrow, nonpolar cavity. 2) Changing the ionization states of the titratable residues by reducing the pH from 7 to 4 in the x-ray crystal structure does not alter the channel-ion potential profile sufficiently to account for the increase in conductance in lowering the pH. Therefore a conformational change in the transmembrane helices of the channel is required for ion conduction. 3) The local friction of ions moving within the channel is similar to that of ions in bulk water. However, the effective mobility in the selectivity filter is smaller due to the partial confinement of ions in the selectivity filter by negative structural charges in the protein (Chiu et al., 1993; Allen et al., 1999). This can be seen in the computed trajectories in Fig. 4, noting that the fluid dynamic diffusion coefficient for ions in the selectivity filter is the same as for ions elsewhere in the channel, but the ions in the selectivity filter are effectively immobilized by the negative charges in the carbonyl oxygens lining the selectivity filter lumen. 4) The most common occupancy state of the open channel at near-physiological concentrations is two ions in the selectivity filter. In and near the selectivity filter are where ion-ion interactions primarily occur. The dominant mode for ion motion through the selectivity filter is effectively by a knock-off mechanism involving three ions, as suggested experimentally (Jiang and MacKinnon, 2000). 5) For near-physiological electrolyte concentrations there is seldom multiple occupancy in the extracellular vestibule or along the intracellular half of the channel. Ion motion in those regions is therefore largely governed by the electrodiffusion of single ions. It is for this reason that the one-dimensional approximation to the motion embodied in the Brownian computational model in this paper gives reasonably accurate estimates of the flux. 6) The overall saturation behavior of the channel in symmetric solutions is rather well fit by a simple model of two resistors in series, one for the selectivity filter and the other for the wider parts of the channel. The resistance of the selectivity filter is $\sim 2 \times 10^9$ Ω. The combined resistance of the wider parts of the channel is approximately inversely proportional to the bath concentration of permeant ions.

Our calculations are generally consistent with other computational studies of the KcsA channel. Our MD trajectories for ions in the selectivity filter and in the wider regions of the channel in general agree with those of other workers (Bernèche and Roux, 2000; Guidoni et al., 2000; Shrivastava and Sansom, 2000) The observation in the BD calculations that the dominant occupancy state in the channel is two ions $\sim$7 Å apart agrees with free energy perturbation studies (Åqvist and Luzhkov, 2000), as well as being also suggested by the x-ray model structure (Doyle et al., 1998). Our ionization state for the residue Glu-71 is somewhat more negatively charged than suggested by others (Roux and MacKinnon, 1999; Åqvist and Luzhkov, 2000), perhaps due to a somewhat different methodology of computing the pK_a. As these residues are over 6 Å from the channel axis and are largely occluded by the selectivity filter from the channel axis, this difference is unlikely to affect the conclusions of this study. We also appear to show somewhat less tendency for an ion to occupy the wide part of the channel than previously suggested (Roux and MacKinnon, 1999). This difference may be due to the fact that our ion distributions are computed for an opened channel. Also, Roux and MacKinnon based their main conclusions on calculations in which the protein was assigned a dielectric constant of 2, whereas our assumed dielectric constant of 20 would somewhat attenuate the effect of the pore helix potentials to attract an ion into the cavity.

In the approach described in this paper, molecular modeling based on structural data, electrostatic calculations, MD, and BD simulations are combined to achieve a comprehensive view of the permeation process in the KcsA ion channel. The same overall approach seems capable of application to other ion channels as well.

This work was supported by the National Science Foundation. Computer time from the National Computational Science Alliance, which is also

largely funded by the National Science Foundation, is gratefully acknowledged. Simulations were carried out on the Origin 2000 at the National Center for Supercomputing Applications at the University of Illinois. We thank Dr. Robin Shealy for preparing the refined KcsA structure and Drs. Shankar Subramaniam, Larry Scott, and Serdar Kuyucak for helpful comments.

REFERENCES

Aidley, D. J., and P. R. Stanfield. 1996. Ion Channels: Molecules in Action. Cambridge University Press, Cambridge, UK.

Allen, T. W., A. Bliznyuk, A. P. Rendell, S. Kuyucak, and S.-H. Chung. 2000. The potassium channel: structure, selectivity and diffusion. *J. Chem. Phys.* 112:8191–8204.

Allen, T. W., S. Kuyucak, and S.-H. Chung. 1999. Molecular dynamics study of the KcsA potassium channel. *Biophys. J.* 77:2502–2516.

Antosiewicz, J., J. A. McCammon, and M. K. Gilson. 1994. Prediction of pH-dependent properties of proteins. *J. Mol. Biol.* 238:415–436.

Åqvist, J., and V. Luzhkov. 2000. Ion permeation mechanism of the potassium channel. *Nature.* 404:881–884.

Bek, S., and E. Jakobsson. 1994. Brownian dynamics study of a multiply-occupied cation channel: application to understanding permeation in potassium channels. *Biophys. J.* 66:1028–1038.

Bernèche, S., and B. Roux. 2000. Molecular dynamics of the KcsA K^+ channel in a bilayer membrane. *Biophys. J.* 78:2900–2917.

Brooks, B. R., R. E. Bruccoleri, B. D. Olafson, D. J. States, S. Swaminathan, and M. Karplus. 1983. CHARMM: a program for macromolecular energy, minimization, and dynamics calculations. *J. Comp. Chem.* 4:187–217.

Chiu, S.-W., J. A. Novotny, and E. Jakobsson. 1993. The nature of ion and water barrier crossings in a simulated ion channel. *Biophys. J.* 64: 98–109.

Chung, S.-H., T. W. Allen, M. Hoyles, and S. Kuyucak. 1999. Permeation of ions across the potassium channel: Brownian dynamics studies. *Biophys. J.* 77:2517–2533.

Cooper, K., E. Jakobsson, and P. Wolynes. 1985. The theory of ion transport through membrane channels. *Prog. Biophys. Mol. Biol.* 46: 51–96.

Corry, B., S. Kuyucak, and S.-H. Chung. 2000. Tests of continuum theories as models of ion channels: II. Poisson-Nernst-Planck theory versus Brownian dynamics. *Biophys. J.* 78:2364–2381.

Cowan, S. W., T. Schirmer, G. Rummel, M. Steiert, R. Ghosh, R. A. Pauptit, J. N. Jansonius, and J. P. Rosenbusch. 1992. Crystal structures explain functional properties of two *E. coli* porins. *Nature.* 358:727–733.

Cuello, L. G., J. G. Romero, D. M. Cortes, and E. Perozo. 1998. pH-dependent gating in the *Streptomyces lividans* K^+ channel. *Biochemistry.* 37:3229–3236.

Doyle, D. A., J. M. Cabral, R. A. Pfuetzner, A. L. Kuo, J. M. Gulbis, S. L. Cohen, B. T. Chait, and R. MacKinnon. 1998. The structure of the potassium channel: molecular basis of K^+ conduction and selectivity. *Science.* 280:69–77.

Farkas, L. 1927. Rate of nucleus formation in saturated vapors. *Z. Physik. Chem. (Leipzig).* 125:236–242.

Gibas, C. J., S. Subramaniam, J. A. McCammon, B. C. Braden, and R. J. Poljak. 1997. pH dependence of antibody/lysozyme complexation. *Biochemistry.* 36:15599–15614.

Gilson, M. K. 1993. Multiple-site titration and molecular modeling: two rapid methods for computing energies and forces for ionizable groups in proteins. *Proteins.* 15:266–282.

Guidoni, L., V. Torre, and P. Carloni. 2000. Water and potassium dynamics inside the KcsA K^+ channel. *FEBS Lett.* 477:37–42.

Hänggi, P., P. Talkner, and M. Borkovec. 1990. Reaction-rate theory: 50 years after Kramers. *Rev. Mod. Phys.* 62:251–341.

Heginbotham, L., M. LeMasurier, L. Kolmakova-Partensky, and C. Miller. 1999. Single *Streptomyces lividans* K^+ channels: functional asymmetries and sidedness of proton activation. *J. Gen. Physiol.* 114:551–559.

Hille, B. 1992. Ionic Channels of Excitable Membranes, 2nd ed. Sinauer, Sunderland, MA.

Hodgkin, A. L., and A. F. Huxley. 1952. A quantitative description of membrane current and its application to conduction and excitation in nerve. *J. Physiol.* 117:500–544.

Hodgkin, A. L., and R. D. Keynes. 1955. The potassium permeability of a giant nerve fibre. *J. Physiol.* 128:61–88.

Huang, C.-J., I. Favre, and E. Moczydlowski. 2000. Permeation of large tetraalkyl ammonium cations through mutant and wild-type voltage-gated Na^+ channels as revealed by relief of block at high voltage. *J. Gen. Physiol.* 115:435–453.

Jakobsson, E. 1998. Using theory and simulation to understand permeation and selectivity in ion channels. *Methods.* 14:342–351.

Jakobsson, E., and S.-W. Chiu. 1987. Stochastic theory of ion movement in channels with single-ion occupancy. *Biophys. J.* 52:33–45.

Jiang, Y., and R. MacKinnon. 2000. The barium site in a potassium channel by x-ray crystallography. *J. Gen. Physiol.* 115:269–272.

Jorgensen, W. L., and J. Tirado-Rives. 1988. The OPLS potential functions for proteins: energy minimizations for crystals of cyclic peptides and crambin. *J. Am. Chem. Soc.* 110:1657–1666.

Killian, J. A. 1998. Hydrophobic mismatch between proteins and lipids in membranes. *Biochim. Biophys. Acta.* 1376:401–416.

Laskowski, R. A., M. W. MacArthur, D. S. Moss, and J. M. Thornton. 1993. PROCHECK: a program to check the stereochemical quality of protein structures. *J. Appl. Crystallogr.* 26:283–291.

Madura, J. D., J. M. Briggs, R. C. Wade, M. E. Davis, B. A. Luty, A. Ilin, J. Antosiewicz, M. K. Gilson, B. Bagheri, L. R. Scott, and J. A. McCammon. 1995. Electrostatics and diffusion of molecules in solution: simulations with the University of Houston Brownian dynamics program. *Comp. Phys. Commun.* 91:57–95.

McQuarrie, D. A. 1976. Statistical Mechanics. Harper Collins, New York. 452–466.

Meuser, D., H. Splitt, R. Wagner, and H. Schrempf. 1999. Exploring the open pore of the potassium channel from *Streptomyces lividans. FEBS Lett.* 462:447–452.

Perozo, E., D. M. Cortes, and L. G. Cuello. 1999. Structural rearrangements underlying K^+ channel activation gating. *Science.* 285:73–78.

Roux, B., and R. MacKinnon. 1999. The cavity and pore helices in the KcsA K^+ channel: electrostatic stabilization of monovalent cations. *Science.* 285:100–102.

Sali, A., J. P. Overington, M. S. Johnson, and T. L. Blundell. 1990. From comparisons of protein sequences and structures to protein modeling and design. *Trends Biochem. Sci.* 15:235–240.

Sancho, M., M. B. Partenskii, V. Dorman, and P. C. Jordan. 1995. Extended dipolar chain model for ion channels: electrostriction effects and the translocational energy barrier. *Biophys. J.* 68:427–433.

Sayle, R. A., and E. J. Milner-White. 1995. RasMol: biomolecular graphics for all. *Trends Biochem. Sci.* 20:374–376.

Schrempf, H., O. Schmidt, R. Kummerlen, S. Hinnah, D. Muller, M. Betzler, T. Steinkamp, and R. Wagner. 1995. A prokaryotic potassium ion channel with two predicted transmembrane segments from *Streptomyces lividans. EMBO J.* 14:5170–5178.

Shrivastava, I. H., C. E. Capener, L. R. Forrest, and M. S. P. Sansom. 2000. Structure and dynamics of K channel pore-lining helices: a comparative simulation study. *Biophys. J.* 78:79–92.

Shrivastava, I. H., and M. S. P. Sansom. 2000. Simulations of ion permeation through a potassium channel: molecular dynamics of KcsA in a phospholipid bilayer. *Biophys. J.* 78:557–570.

Singh, C., R. Sankararamakrishnan, S. Subramaniam, and E. Jakobsson. 1996. Solvation, water permeation, and ionic selectivity of a putative model for the pore region of the voltage-gated sodium channel. *Biophys. J.* 71:2276–2288.

Smart, O. S., J. M. Goodfellow, and B. A. Wallace. 1993. The pore dimensions of gramicidin A. *Biophys. J.* 65:2455–2460.

Splitt, H., D. Meuser, I. Borovok, M. Betzler, and H. Schrempf. 2000. Pore mutations affecting tetrameric assembly and functioning of the potassium channel KcsA from *Streptomyces lividans*. *FEBS Lett.* 472:83–87.

Stampe, P., J. Arreola, P. Pérez-Cornejo, and T. Begenisich. 1998. Non-independent K^+ movement through the pore in IRK1 potassium channels. *J. Gen. Physiol.* 112:475–484.

Tanford, C., and R. Roxby. 1972. Interpretation of protein titration curves: application to lysozyme. *Biochemistry.* 11:2192–2198.

Terlau, H., H. Boccaccio, B. M. Olivera, and F. Conti. 1999. The block of *Shaker* K^+ channels by κ-conotoxin PVIIA is state dependent. *J. Gen. Physiol.* 114:125–140.

van Gunsteren, W. F., S. R. Billeter, A. A. Eising, P. H. Hünenberger, P. Krüger, A. E. Mark, W. R. P. Scott, and I. G. Tironi. 1996. Biomolecular Simulation: The GROMOS96 Manual and User Guide. vdf Hochschulverlag, Zürich.

Wall, M. E., S. Subramaniam, and G. N. Phillips, Jr. 1999. Protein structure determination using a database of interatomic distance probabilities. *Protein Sci.* 8:2720–2727.

Zhou, M., J. H. Morais-Cabral, S. Mann, and R. Mackinnon. 2001. Potassium channel receptor site for the inactivation gate and quaternary amine inhibitors. *Nature.* 411:657–661.

APPENDIX B
Three-Dimensional Continuum Simulations of Ion Transport Through Biological Ion Channels: Effect of Charge Distribution in the Constriction Region of Porin

Journal of Computational Electronics 1: 335–340, 2002

Three-Dimensional Continuum Simulations of Ion Transport Through Biological Ion Channels: Effect of Charge Distribution in the Constriction Region of Porin

T.A. VAN DER STRAATEN, J. TANG AND R.S. EISENBERG
Department of Molecular Biophysics and Physiology, Rush Medical College, 1750 W. Harrison St., Chicago, IL 60612, USA
trudyv@uiuc.edu
jtang@rush.edu
beisenbe@rush.edu

U. RAVAIOLI AND N.R. ALURU
Beckman Institute for Advanced Science and Technology, University of Illinois at Urbana-Champaign, 405 N. Mathews Ave., Urbana, IL 61801, USA
ravaioli@uiuc.edu
aluru@uiuc.edu

Abstract. Drift-diffusion models are useful for studying ion transport in open protein channel systems over time scales that cannot be resolved practically by detailed molecular dynamics or quantum approaches. Water is treated as a uniform background medium with a specific dielectric constant and macroscopic current flow is resolved by assigning an appropriate mobility and diffusivity to each ionic species. The solution of Poisson's equation over the entire domain provides a simple way to include external boundary conditions and image force effects at dielectric discontinuities. Here we present a 3-D drift-diffusion model of ion (K^+ and Cl^-) permeation through the porin channel *ompF*, and its mutant *G119D*, implemented using the computational platform PROPHET.

Keywords: ion channels, Poisson-Nernst-Planck, transport simulation, *ompF* porin, nanotechnology

1. Introduction

Ion channels are a class of proteins that form nanoscopic aqueous tunnels to control the passage of ions through the otherwise almost impermeable membranes of all biological cells. Each channel consists of a chain of amino acids carrying a strong and rapidly varying localized charge. From a biological point of view, ion channels maintain the correct internal ion composition that is crucial to cell survival and function. They directly control electrical signaling in the nervous system, muscle contraction, and the delivery of many clinical drugs (Hille 1992). There are many types of ion channels, each with a specialized function. Some channels have the ability to selectively transmit or block a particular ion species and many exhibit switching properties similar to nanoscale electronic devices.

ompF is a trimeric porin channel that resides in the outer membrane of the *e-coli* bacterium. Its well-known and extremely stable molecular structure make it a good choice for experimental and computational studies. Each monomer appears to operate independently, making it a possible candidate for multilevel logic devices. *ompF* carries a net negative charge of approximately $-30|e|$, where e is the electron charge, and is moderately selective for cations. The narrow constriction region of each hourglass-shaped channel is highly charged due to the presence of three positively charged

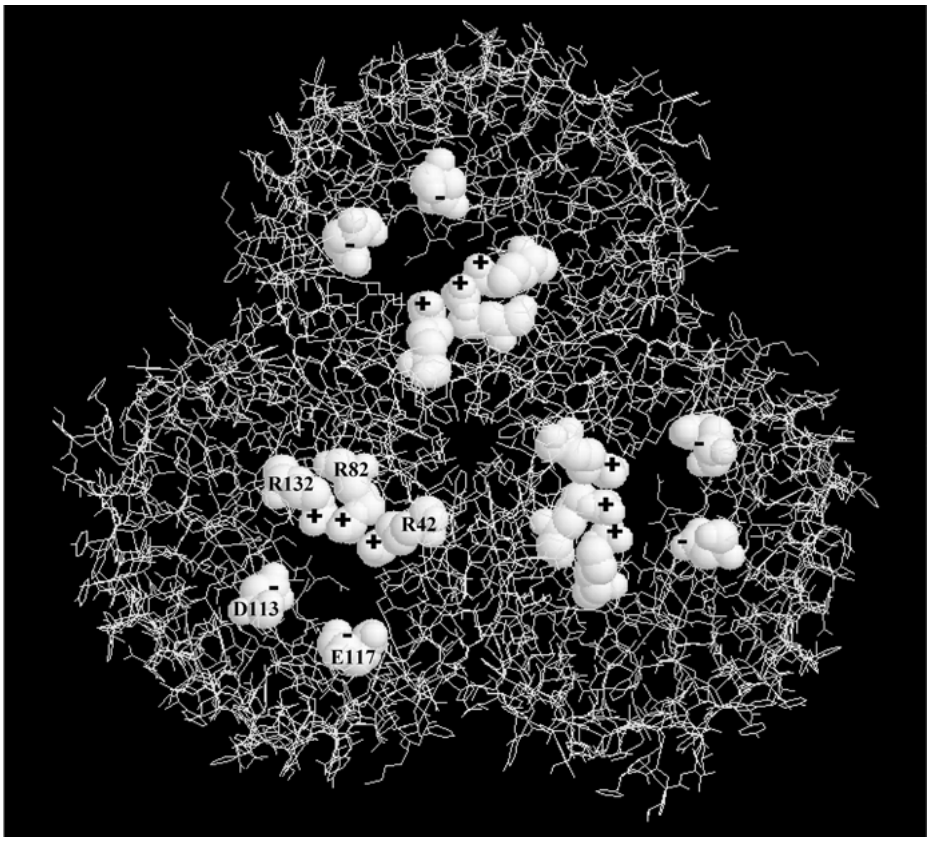

Figure 1. Molecular structure of *ompF*, projected along the length of the channel, showing the three-fold symmetry of the trimer. The five ionized amino acids in the constriction region of each pore are highlighted.

(R42, R82, R132) and two negatively charged (*D113*, *E117*) amino acids (Phale *et al.* 2001), as shown in Fig. 1. The arrangement of these charges gives rise to a very strong electric field parallel to the plane of the membrane, which is believed to govern the behavior of the open channel. *ompF* can be mutated by replacing or deleting one or more of the amino acids, thus altering the charge distribution along the channel. Engineering channels with specific conductances and selectivities is thus conceivable. The mutant *G119D*, formed by replacing an uncharged amino acid (glycine) with a negatively charged aspartate, has a structure almost unchanged from that of *ompF* yet its conductance is measured to be between 15% and 50% lower than *ompF*, depending on the concentration of the salt solution in which it is immmersed. Though the overall structure of the porin is not compromised by this mutation the constriction region becomes significantly narrower due to the bulk and orientation of the aspartate. The observed reduction in channel conductance is believed to be a result of changes in both the steric and electrostatic environment of the pore constriction.

Here we describe a three-dimensional (3-D) drift-diffusion model of ion (K^+ and Cl^-) permeation through *ompF* and its mutant *G119D*, implemented using the computational platform PROPHET (http://www-tcad.stanford.edu/). While continuum models sacrifice resolution of molecular detail they can be used to compute macroscopic current with a reasonable amount of computational effort and have been found to describe permeation through ion channels surprisingly well (Hollerbach *et al.* 2000). Using this approach we investigate the effect of the charge distribution in the pore constriction on the open channel conductance and selectivity. In Section 2 we describe our model; in Section 3 we present the results, in particular we compare the current-voltage characteristics and selectivities of *G119D* and *ompF*. Section 4 concludes with a brief discussion of this work and future plans.

2. Poisson-Drift-Diffusion Model

The channel system studied here is comprised of a porin trimer in situ in a cell membrane, immersed in an aqueous bath of KCl. Experimentally it is possible to maintain different salt concentrations on either side of the membrane (hereafter referred to as C_{left} and C_{right}). Electrodes are immersed in the baths to apply a fixed bias across the channel/membrane system. The electrostatic environment of the channel is determined by (i) mobile ions permeating through the open channel, (ii) fixed (permanent) charges that reside on the protein itself, and (iii) the charges in the aqueous baths and on the electrodes. The local electrostatic potential φ is related to all the charges in the system by Poisson's equation,

$$\nabla \cdot (\varepsilon \nabla \varphi) = -(\rho_{fixed} + \rho_+ + \rho_-) \tag{1}$$

where ε is the dielectric constant, and ρ_{fixed}, ρ_+ and ρ_- are the charge densities per unit volume of fixed charges residing on the protein, K^+ ions and Cl^- ions, respectively. Current flow $\vec{j}_\pm$ is described by the drift-diffusion equation

$$\vec{j}_\pm = -(\mu_\pm \rho_\pm \nabla \varphi \pm D_\pm \nabla \rho_\pm) \tag{2}$$

where $\mu_\pm$ and $D_\pm$ are, respectively, the mobilities and diffusivities of the ionic species. Conservation of charge dictates

$$\nabla \cdot \vec{j}_\pm + \frac{\partial \rho_\pm}{\partial t} = S_\pm \tag{3}$$

where $S_\pm$ can be any form describing the details of ion binding and other chemical phenomena that populate or deplete the ion densities. In the present model we do not consider such phenomena and set $S_\pm = 0$. We seek a steady-state solution for φ, ρ_+ and ρ_-that simultaneously satisfies Eqs. (1)–(3) subject to specific Dirichlet boundary conditions at the electrodes (C_{left}, C_{right} and V_{bias}).

The model described above was implemented using the PROPHET simulator, a computational platform originally developed at Lucent Technologies and currently being extended at Stanford University. The PROPHET simulator uses the "dial-an-operator" methodology to construct systems of partial differential equations by combining existing differential operators described using a scripting syntax. Equations (1)–(3) and the boundary conditions are constructed using existing PROPHET operators. After the channel geometry is defined on a customized mesh provided by the user, the equations are discretized and the linear system is solved using iterative methods. Physical parameters are assigned to the different regions of the domain at run-time. For the results presented here we use $\varepsilon = 80$, 20 and 2, for the aqueous, protein and membrane regions, respectively. Diffusivities were chosen to fit measured current-voltage (I-V) curves, assuming $D_+ = D_-$, and mobilities were assigned using the Einstein relations, reducing the number of adjustable parameters to one.

The distribution of charge on each amino acid is modelled by associating a fractional point charge (in units of $|e|$) to each atom. Values for these charges in neutral solutions are calculated using *ab initio* quantum chemistry codes. For this work we have used the tabulated OPLS partial charges, a force field used widely in molecular dynamics simulations of protein molecules (Jorgensen and Tirado-Rives 1988).

3. Results

As mentioned in the previous section, the distribution of permanent charge around each amino acid is obtained from quantum chemistry calculations that treat each amino acid as a free entity in solution. The dielectric environment and proximity of neighboring ionized amino acids in the folded protein is expected to alter the charge distribution. Electrostatic calculations by Karshikoff *et al.* (1994) suggest that at neutral pH the charges on amino acids R82, located inside the constriction region, and R167, located near the mouth of the channel, should be scaled down from +1 to zero (Dutzler private communication). More recent calculations (Schirmer and Phale 1999, Varma and Jakobsson private communication) however, indicate that both R82 and R167 should in fact be fully ionized at neutral pH. Since both R82 and R167 line the pore of the channel it is important that these charges be properly represented. Figure 2 shows I-V curves computed for symmetric bath concentrations of (a) 100 mM KCl and (b) 1 M KCl, with both representations of the charge distribution: R82, R167 uncharged—solid symbols; R82, R167 fully ionized—open symbols. Figure 2(c) shows the computed I-V curve for a system with 100 mM KCl on one side of the membrane and 1 M KCl on the other, assuming R82 and R167 are uncharged. A diffusivity in the range $(0.8\text{–}1.02) \times 10^{-5}$ cm^2 s^{-1} provides a satisfactory fit to the experimental data. Interestingly, the extra positive

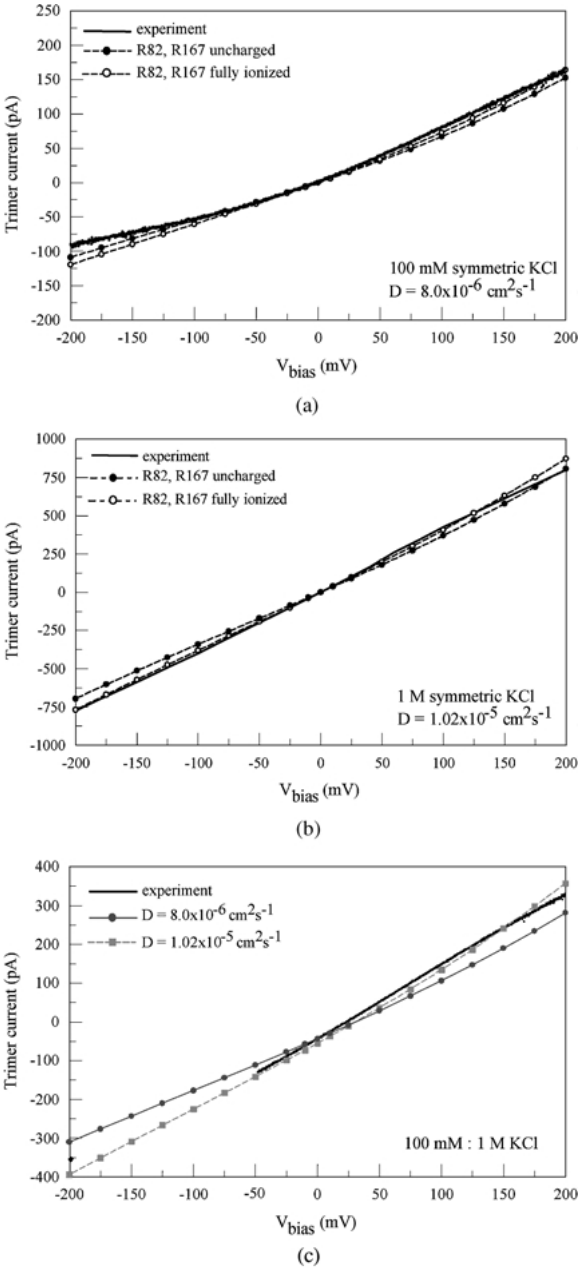

Figure 2. Comparison of drift-diffusion model with experimental *I-V* curves for *ompF* in (a) 100 mM (b) 1 M and (c) 100 mM : 1 M KCl. Simulations run with both R82 and R167 fully ionized are indicated with open circles.

charge on the protein does not make a significant difference to the open channel conductance. However the selectivity of the *ompF* for cations, defined here as the fraction of total current carried by cations, is reduced from 66% to 62% at 1 M KCl, and 88% to 84% at

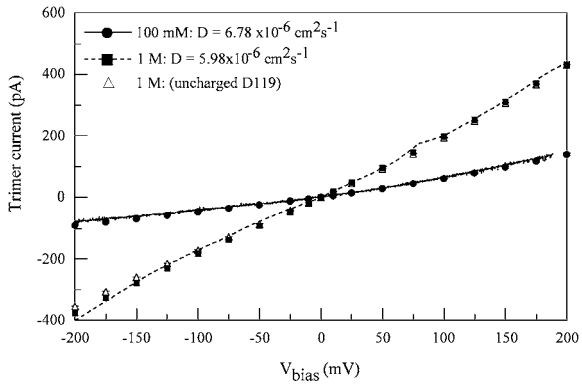

Figure 3. Comparison of drift-diffusion model with measured *I-V* curves for *G119D* in 100 mM and 1 M KCl. Measured data are indicated with solid (100 mM) and dashed (1 M) lines, the simulation data are indicated with symbols.

100 mM KCl, which consistent with the addition of $+6|e|$ making the channel less electrostatically accessible to cations. These values are commensurate with the value 77% measured for 100 mM – 1 M KCl (Schirmer and Phale 1999).

G119D is created by replacing the neutral glycine, *G119*, tucked between the aspartate *D113* and glutamate *E117* (see Fig. 1), both negatively charged, with an aspartate *D119*, also negatively charged. In addition to increasing the negative charge the bulkier aspartate also reduces the volume available for ions to pass through the constriction zone. Figure 3 shows the measured and computed *I-V* characteristics for *G119D*. At l00 mM KCl the conductance is about 15% lower than that of *ompF*, while at 1 M the conductance of *G119D* is about 40% lower. A diffusivity in the range (6.0–6.8) $\times$ 10^{-6} cm^2 s^{-1} is able to fit a fairly large range of experimental data. The simulations predict *G119D* to be more cation selective than *ompF* (69% at 1 M and 90% at 100 mM KCl), as would be expected from the addition of an extra charge in the constriction region.

The mutation introduces both steric and electrostatic changes in the constriction region of the channel. However, the relative contribution of each change to the reduced conductance observed in *G119D* is not known. Understanding the relationship between structure and function of ion channels is crucial if new channels are to be designed with specific properties and behaviors. Simulations can perhaps find their greatest use in providing insight that cannot be measured or inferred from experiment. As an example of this we have attempted to separate the steric and electrostatic effects in *G119D* by scaling down the charge distribution on the aspartate

to zero. This creates a channel (albeit, a virtual one) that should be electrostatically similar to *ompF* but structurally the same as *G119D*. Simulations at 1 M KCl reveal that the conductance (shown in Fig. 3) of such a channel, were it to exist, is almost the same as *G119D* despite the difference in the charge constellation in the constriction region. The selectivity, on the other hand, reduces to 56%. This raises the question of whether the lowered conductance of *G119D* is more the result of a narrowing of the pore constriction than any electrostatic changes. One issue that needs further probing is how the orientation of the key amino acids in constriction region depends on the local field. If it were possible to remove the charge on the aspartate would the charged amino acids reorient in such a way that the channel cross-section is appreciably altered? Detailed molecular dynamics simulations are required to answer these types of questions. An interesting mutation to consider experimentally would be *G119N* where the uncharged glycine is replaced with an asparagine, to emulate the bulk of the aspartate without the charge. If the above conjecture is correct then the conductance of *G119N* should be similar to *G119D* and its selectivity similar to *ompF*.

Ion occupancies, defined as the integral of the ion density over a specified volume, have been calculated for *ompF* and *G119D*, for a range of salt concentrations and applied bias. The latter has very little effect on the predicted ion occupancies, since the effective fixed charge lining the pore is so strong. Figure 4 compares the cation and anion occupancies for the four channel scenarios discussed above, computed for the conditions of zero applied potential and 1 M KCl. In all four cases, occupation of the constriction region is more favorable for cations, and the predicted changes in occupancy upon mutation are consistent with the changes in the net charge in the pore constriction.

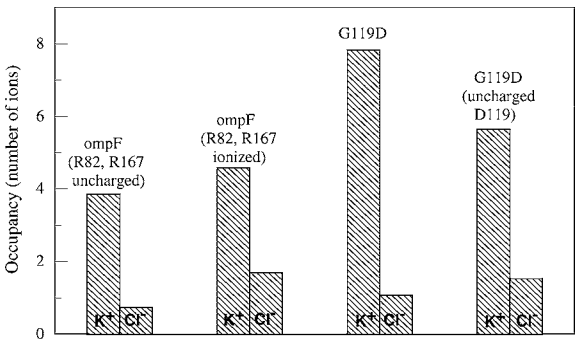

Figure 4. Effect of adding or deleting charges in the channel constriction on the cation and anion occupancies.

Conclusion

The success of the drift-diffusion theory in predicting measured *IV* curves of *ompF* and *G119D* is reasonably good considering that we have used only one adjustable parameter (diffusivity) to simulate ion permeation in a wide range of experimental conditions. The calibrated diffusivities agree to within a factor of 3 with the experimentally measured values in bulk salt solution. Theoretical values for the ion diffusivities inside the porin channel, as calculated from molecular dynamics simulations, also agree with the calibrated values to within 20%. Clearly a uniform diffusivity cannot capture all the physical effects affecting ion transport in an inherently three-dimensional restricted and highly charged volume. The development of a diffusivity model for each ionic species that includes a dependence on position (or local field) and/or ion density is the subject of ongoing work.

Acknowledgments

This work was partially supported by the NSF Distributed Center for Advanced Electronics Simulation (DesCArtES) grant ECS 98-02730, DARPA contract N65236-98-1-5409 (B.E.) and an NSF KDI grant to the University of Illinois. The authors thank E. Jakobsson and the staff of the Computational Biology group at the University of Illinois for useful discussions, and R.W. Dutton, Z. Yu and D. Yergeau of Stanford University for assistance with implementation of PROPHET applications. The authors also gratefully acknowledge Tilman Schirmer (Biozentrum, University of Basel) and Raimund Dutzler (Rockefeller University) for providing the crystallographic structures for *ompF* and *G119D*.

References

Chiu S.W. and Jakobsson E. Private communication.

Dutzler R. Private communication.

Hille B. 1992. Ionic Channels of Excitable Membranes. Sinauer Associates Inc., MA.

Hollerbach U., Chen D.P., Busath D.D., and Eisenberg B. 2000. Predicting function from structure using the Poisson-Nernst-Planck equations: Sodium current in the gramicidin a channel. Langmuir 16: 5509–5514.

Jorgensen W.L. and Tirado-Rives J. 1988. J. Am. Chem. Soc. 110: 1657–1666.

Karshikoff A., Spassov V., Cowan S.W., Ladenstein R., and Schirmer T. 1994. J. Mol. Biol. 240(4): 372–384.

Phale P.S., Philippsen A., Widmer C., Phale V.P., Rosenbusch J.P., and Schirmer T. 2001. Role of charged residues at the *ompF* porin channel constriction probed by mutagenesis and simulation. Biochemistry 40: 6319–6325.

Schirmer T. and Phale P.S. 1999. Brownian dynamics simulation of ion flow through porin channels. J. Mol. Biol. 294: 1159–1167.

Varma S. and Jakobsson E. Private communication.